In-Situ Probing of the Surface Properties of Droplets in the Air

Jesse B. Brown[#1], Yuqin Qian[#1], Zhi-Chao Huang-Fu[1], Tong Zhang[1,2], Hui Wang[1], and Yi Rao*[1]

[1]Department of Chemistry and Biochemistry, Utah State University, Logan, UT 84322

[2]Institute of Chemistry, Chinese Academy of Sciences, Beijing 100190, China

Abstract

Surface properties of nano-droplets and micro-droplets are intertwined with their immense applicability in biology, medicine, production, catalysis, the environment, and the atmosphere. However, many means for analyzing droplets and their surfaces are destructive, non-interface specific, not conducted under ambient conditions, require sample substrates, conducted *ex situ*, or a combination thereof. For these reasons, a technique for surface-selective *in situ* analyses under any conditions is necessary. This feature article presents recent developments in second-order nonlinear optical scattering techniques for *in situ* interfacial analysis of aerosol droplets in the air. First, we describe the abundant utilization of such droplets across industries and how their unique surface properties lend to their ubiquitous usage. Then, we describe the fundamental properties of droplets and their surfaces followed by common methods for their study. We next describe the fundamental principles of sum-frequency generation (SFG) spectroscopy and the Langmuir adsorption model, and how they are used together to describe adsorption processes at liquid and droplet surfaces. We also discuss the history of developments of second-order scattering from droplets suspended in dispersive media and introduce second-harmonic scattering (SHS) and sum-frequency scattering (SFS) spectroscopies. We then go on to outline the developments of SHS, electronic sum-frequency scattering (ESFS), and vibrational sum-frequency scattering (VSFS) from droplets in the air and discuss the fundamental insights about droplet surfaces that the techniques have provided. Lastly, we describe some of the areas of nonlinear scattering from airborne droplets which need improvement, as well as potential future directions and utilizations of SHS, ESFS, and VSFS throughout environmental systems, interfacial chemistry, and fundamental physics. The goal of this article is to spread knowledge about droplets and their unique surface properties as well as introduce second-order nonlinear scatterings to a broad audience who may be unaware of recent progresses and advancements in their applicability.

*Corresponding author: yi.rao@usu.edu

[#]Those authors contributed equally to this work.

Introduction

Nano- and micro-droplets and particles are of ubiquitous importance across the sciences from biology to catalysis, and atmospheric and environmental sciences owing largely to their surface characteristics.[1] Considering the size range of tens of nanometers to a few micrometers in diameter, these sub-femtoliter systems have properties which are distinct from their macroscopic counterparts, and their surface properties are unique compared to their underlying bulk. Here, we define the surface (and surface properties) to only include the outer few monolayers of a material. For this reason, such droplet species cannot be approximated by macroscopic systems and surface properties cannot be approximated by bulk properties. The unique properties of nano-droplets/micro-droplets and their surfaces not only have led to their use in biomarkers, imaging, drug delivery, synthesis, and catalysis, but also impact the environment and animal well-being by way of aerosol particles and the exceptional surface/interfacial physical and chemical properties which govern their atmospheric activity. The terms "surface" and "interface" may be used interchangeably throughout this article.

Surfaces of nano- and micro-droplets have shown promise in biological and medical applications made possible by their surfactant-rich surfaces. Demonstrating utility in biology and medicine, ultrasonic phase-shifting nano-droplets can provide precise drug delivery and imaging contrast agents. These droplets are composed of a semi-solid surface, made from lipids, proteins, or polymers, and a liquid perfluorocarbon-based interior that can be loaded with chemicals specific to the droplet's desired task which will vaporize under ultrasonic radiation. The size of the droplets, tens of nanometers to a few micrometers, allows precise spatial targeting and accumulation, while the ultrasonic radiation provides enhanced drug delivery through both vaporization of the droplet and inducing pore formation in membranes.[2] Based on the same concept of controlled vaporization in hard-to-reach areas, droplet occlusion may hold promise for producing bubbles which block blood flow to tumors.[1] These employments of droplets in ultrasonic imaging and therapeutics are made possible by their surfaces which are made of surfactants. The surfactant shell stabilizes the perfluorocarbon droplet within, allows the formation of a stable emulsion by increasing the surface tension between the core and surrounding aqueous medium, and provides the appropriately sized droplets.[3] This stabilizing surface allows for easy passage of the droplet through the vascular system and can then be disposed of by the body after the droplet has ruptured. The introduction of droplets into ultrasound systems has further increased its efficiency and usefulness by facilitating intravascular ablation with pinpoint accuracy.[4] Droplets with a surfactant surface and vaporizable liquid core have revolutionized ultrasonic imaging and targeted drug delivery in medicine, which would not be possible without unique surface characteristics holding it all together.

Surfaces of nano- and micro-droplets also hold merit in catalysis and synthesis. Chemical reactions in droplets and at their surfaces have been shown to proceed at rates that are orders of magnitude higher than in bulk solution, owing to easier concentration of reagents and fast diffusion. [5]For instance, the reactive production of H_2 nano-bubbles at the surface of submicron to several micron-sized micro-droplets demonstrated an accelerated production rate over the bulk solution with an inverse relationship between droplet diameter and reaction rate.[6] Many types of chemical reactions have shown acceleration under droplet conditions, from additions, eliminations, and substitution reactions to synthesis steps and redox processes.[7] Causes for such increased reactivity are multifaceted. Partial solvation at droplet surfaces is thought to be an enthalpic intermediate between gas and liquid bulk phase reactions, partially explaining

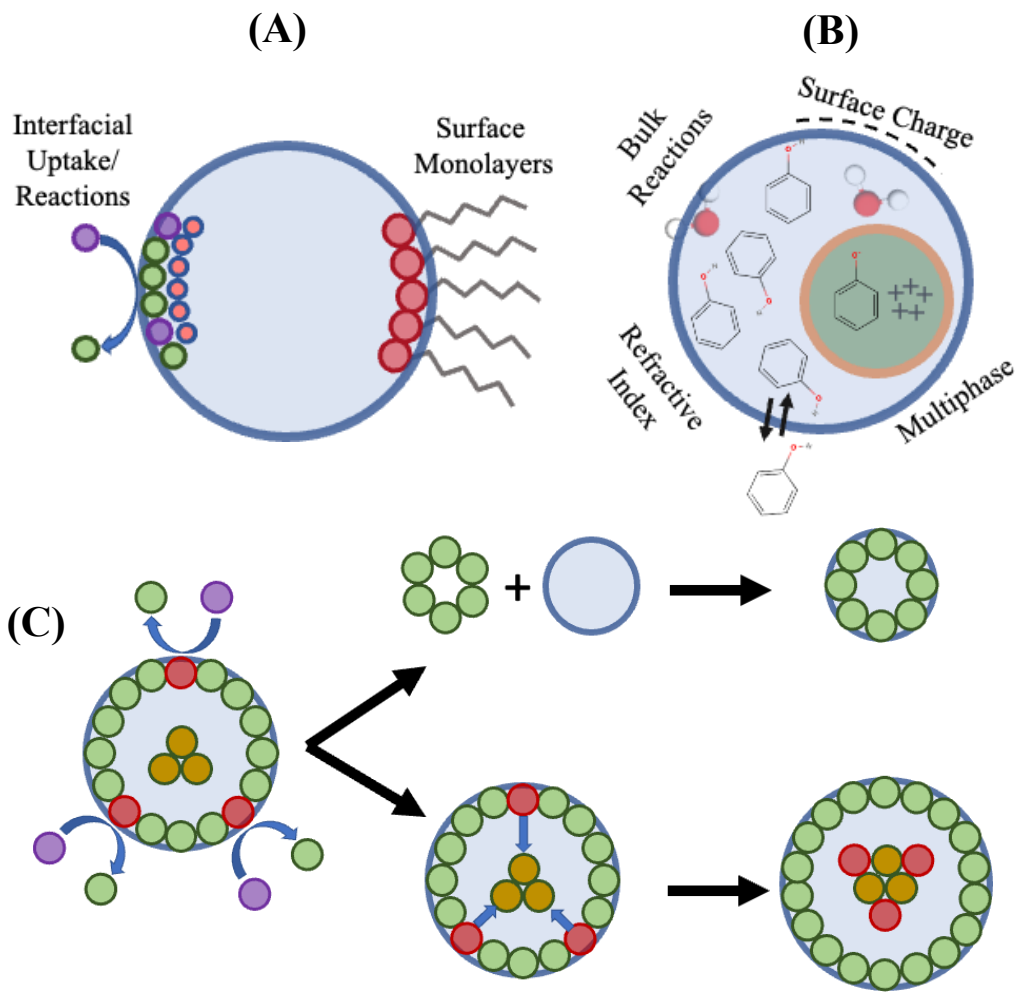

Figure 1. Illustrations of (A) droplet surface properties: the process of interfacial uptake and presence of interfacial monolayers; (B) droplet bulk properties: particle bulk can contain different phase states, bulk reactions and constituents can impact particle surface charge and overall refractive index (phenolate molecules are given as an example); and (C) aerosol surface reactions can result in volatile species which can form new aerosols and nonvolatile species that can contribute to particle growth.

accelerated rates.[8] Additionally, decreasing the size of the droplet and increasing its diffusion coefficient can enhance reaction rates over the bulk solution.[7] Entropic effects can also accelerate or facilitate reactions in small droplet systems which are otherwise thermodynamically forbidden in bulk solutions. At the surface of droplets, molecular ordering decreases entropy and thereby enhances free energy, overcoming this thermodynamic barrier.[9] Especially important for droplets in air like atmospheric aerosols or those generated in spray analysis techniques, are reaction enhancements caused by particle concentration from evaporation.[10] This effect can be increased further for smaller droplets for which diffusion and relative evaporation rates increase. The utilization of droplets in synthesis and catalysis processes has provided fundamental insight to both interfacial chemical mechanisms and the physical properties of droplet surfaces alike, many of which with implications in aerosol chemistry in the atmosphere.

Nano- and micro-droplet surfaces are fundamentally intertwined with atmospheric chemistry through aerosols which govern heterogeneous atmospheric chemical reactions and cloud nucleation, directly impacting climate and environmental health.[11] Some of the unique properties of aerosol droplets are illustrated in Figure 1. The surface of aerosol droplets facilitates important processes of evaporation and condensation, which can affect solute concentration and surface tension of the droplet.[12] The droplet surfaces also host amphiphilic species like fatty acids from organic processes that can form monolayers which encapsulate the droplet and restrict transport through the gas/aerosol droplet interface.[13] Similarly, surface-active molecules can facilitate heterogenous reactions at the gas/aerosol droplet interface (see Figure 1(A)). The underlying bulk of aerosol droplets also impacts its overall physical properties such as refractive index and other optical properties.[14] The aerosol bulk can host in-particle reactions, result in surface charge localization, and can be multiphase in nature with a solid or semisolid organic core[15] (see Figure 1(B)). With the complex nature and properties of aerosol processes, they have been studied extensively.

Atmospheric aerosols of organic origins fall into two overarching categories: primary organic aerosols that are directly emitted into the atmosphere through natural and anthropogenic emissions, and secondary organic aerosols (SOA) which are formed through heterogeneous and multiphase oxidations and condensations of primary organic aerosols.[16] Such secondary species affect climate chemistry by influencing relative humidity and atmospheric pH, scattering and absorbing solar radiation, and altering ice crystal and cloud nucleation.[17] Reactions of SOAs contribute to the overall growth and multiplication of aerosols via heterogeneous oxidation at the gas/particle interface, and through reactions in the dry or aqueous bulk phase of the particle's core. Photocatalytic or radical heterogeneous oxidation of organics present at the surface of an aqueous aerosol particle may result in soluble products which are taken into the particle bulk while less soluble gas-phase products are lost to the atmosphere through the gas/droplet interface and are available to form new SOAs. Further radical and oligomerization reactions in the aqueous bulk phase may then yield products which migrate to the gas/particle interface to continue the growth cycle.[18] This process of particle growth and multiplication is illustrated in Figure 1(C). In addition to their effects on the atmosphere and human health, aerosol droplets and particles are fascinating due to their surface properties which can differ considerably from their bulk, including viscosity, partitioning rates, surface tension, pH, and charging which invoke interesting atmospheric implications.[19] Viscosity and partitioning rates mitigate overall chemical mobility within the particle and at its interface, directly affecting its properties of pH, uptake rates, and charge distribution. The charged surfaces of aerosol particles due to increased ionic activity facilitates adsorption and further solute activity at the interface.[17, 20] An important parameter when considering aerosol droplet properties is the size, which can affect many properties of the droplets stemming from the effects of size on surface tension and therefore interfacial activity as well as the surface area to volume ratio giving rise to mass-limitations.

Some of the unique surface and bulk properties of aerosol droplets are directly caused by their minute scale. A rough calculation shows us that for droplets with diameters of 10 nm, 100 nm, and 1 μm, a single droplet contains on the order of 1.7×10^4, 1.7×10^7, and 1.7×10^{10} water molecules, respectively. This relationship is intuitive, however, such a change in size contributes to rapid change in the surface area to volume ratio, which becomes important when considering surface coverage of a solute for a droplet of mixed composition (see Figure 2). Now, let us consider

an aqueous droplet containing 0.5 M butyric acid, a simple carboxylic acid which is used in food as flavoring additive to resemble butter or cheese. For a droplet with 1 μm diameter, there are enough butyric acid molecules within the 0.5 femtoliter droplet to form an interfacial monolayer of coverage 25-times over, assuming a surface coverage of $2 \times 10^{14} \mathrm{cm}^{-2}$.[21] However, when the droplet diameter is reduced to 100 nm, nearly half of the available molecules would be required to form a surface monolayer. Moreover, a four-fold increase in concenration would be necessary to provide surface monolayer coverage on a 10 nm diameter droplet. For these reasons, surface sensitive studies of droplets with known size distributions are necessary. Additionally, the diameter of liquid droplets can directly effect their surface tension.

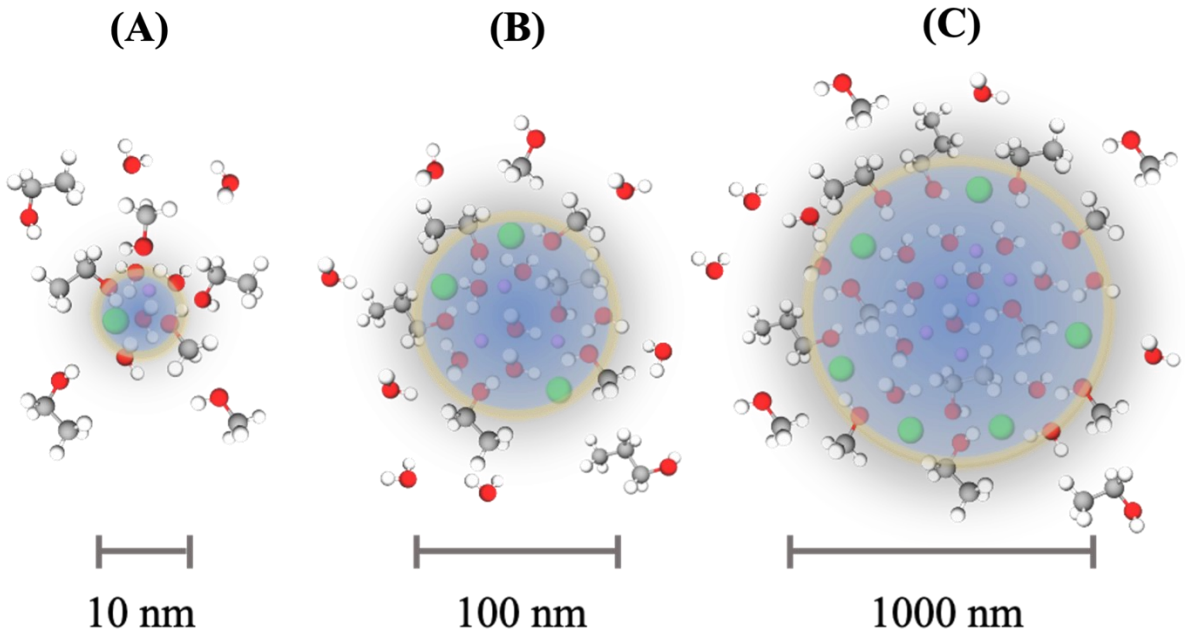

Figure 2. Schematic of aerosol droplets containing water, n-alcohol molecules, and sodium (purple) and chloride (green) at their surfaces and within the underlying bulk for 10 nm(A), 100 nm (B), and 1000 nm (C) species. Depiction is not to scale.

The small nature of nano-droplets and particles not only has an impact on surface converages, but the surface tension of small volume droplets is a factor which changes with droplet size. Based on the original assessment by Gibbs, Tolman confirmed in 1949 that droplet surface tension decreases with droplet radius,[22] which has since been modeled extensively for systems smaller than 10 nm in diameter.[23] For systems of droplets in the air, ambient humidity is a key determining factor in particle size. Given the preditions of Tolman and other groups, one may expect the hygroscopic growth of aerosol droplets to lead to an increase in surface tension. In fact, this phenomenon was demonstrated using atomic force microscopy (AFM) and spectroscopy for droplets of differing compositions.[24] It was found that while droplets containing sodium chloride exhibit a decrease in surface tension with increasing relative humidity and hygroscopic growth, the oposite was the case for droplets containing organic acids. In this case, the mixed composition of the droplets results in solute dilution upon delequecence which also has its own affect on surface tension. Although AFM provided surface tension measurements for the submicron droplets in these experiments, the experiments require the droplets to reside on a substrate which can effect

their mophology and ability to uptake water. For these reasons, an *in situ* analysis of the effects of ambient humidity on the surface properties of airborne droplets with different salt and organic concentrations is desireable. However, both droplet size and surface tension have an impact on interfacial adsorption and uptake.

Studies of Aerosol Droplet Surfaces.

Airborne droplets or particles, aerosols, are especially interesting from a surface perspective as the surrounding medium has less effect on the surface properties if both phases are at equilibrium. Early studies of aerosol droplets and particles were mostly concerned with overall properties like size and concentration.[25] However, we are concerned with aerosol surface properties in this article. Methods for studying aerosol surfaces can be classified in to overarching categories: *ex situ* observations which include all off-line measurements of collected stationary particles, and *in situ* observations which probe droplet and particle properties as they float in air. Before discussing *in* and *ex situ* surface measurements, we must first define the terms "surface specific" or "surface selective." For the purposes of this article, such terms are reserved for techniques which inspect the outer few monolayers of a surface or interface. Such methods include, but are not limited to, SHG and SFG which are forbidden from centrosymmetric bulk under the dipole approximation,[26] AFM,[27] surface enhanced Raman scattering (SERS),[28] X- ray reflectivity,[29, 30] and X-ray photoemission which has a probe depth of several nanometers.[31] Other methods which depend on experimental conditions to be surface sensitive, such as laser microprobe mass spectrometry (LAM-MS) with a probe depth of around 100 nm,[32] are considered to be circumstantially surface sensitive for the purposes of this article.

Mass spectrometry (MS) was one of the first methods for studying impacted aerosol surfaces by way of LAM-MS, which uses laser pulses to fragment molecules at the surface of aerosols which have been collected on a substrate.[33] Being an *ex-situ* technique, LAM-MS requires that the samples be deposited, transported, and stored before analysis which can significantly affect the surface properties of the aerosols through evaporation, reactions, and aging.[25] This is an inherent problem with *ex-situ* analyses. As noted above, AFM has been used to directly measure the surface tension of impacted aerosol droplets.[12] Surface enhanced Raman scattering (SERS) spectroscopy, a surface-sensitive method, has been applied to identifying molecular species from a single aerosol particle,[34] but still requires the particles to be deposited on a substrate. Interesting microscopy/spectroscopy solutions have been developed to probe aerosol surface and bulk properties while simultaneously imaging submicron particles, overcoming the optical diffraction limit. In such instruments, AFM or Raman scattering techniques were combined with photothermal IR spectroscopy (AFM-PTIR and O-PTIR, respectively) and provide vibrational spectroscopic features from the surface and bulk with impressive spatial resolution.[35] However, these techniques are not inherently surface sensitive and still require aerosols to be impacted on a substrate. High-energy, surface-specific X-ray spectroscopies have also been used to probe the surface of aerosols and their reactions.[36] For example, X-ray photoemission combined with aerosol mass spectrometry was used to study interfacial uptake and reduction of viscous aerosol particles.[37] Additionally, X-ray microscopy was used to show that the surface of aerosols can focus incident radiation onto the opposite surface and enhance photochemical reactions.[14] Sum-frequency generation (SFG) spectroscopy, which is inherently surface sensitive, has also been applied to the *ex-situ* analysis of aerosol particles.[38, 39] These studies provided valuable information about aerosol surface properties and compositions, and the technique was also extended to include size resolution.[40] SFG has also been used to study model aerosol systems at the air/liquid interface.[41-43] An exhaustive list of

applications of SFG to atmospheric systems is not given here as it is outside the scope of this article due to the differences in experimental samples. Furthermore, SFG was combined with Raman microscopy to provide a comprehensive view of impacted aerosol particles.[44] These *ex-situ* methods of analyzing aerosol droplet and particle surfaces have contributed to our knowledge about this unique system; however, they require that aerosols be collected onto a substrate which can affect their properties such as available surface area for heterogenous processes and deformation of morphology,[45] and not all such techniques are conducted under atmospherically relevant conditions. Thus, the ideal method for studying aerosol surfaces is *in-situ* under ambient conditions.

An early *in-situ* observation of aerosol surface properties used laser desorption ionization to selectively ionize aerosols at variable depth.[46] This method was similar to LAM-MS mentioned above, but was conducted on laboratory generated particles in air. Even though this method has some surface selectivity, it is not inherently surface-selective and therefore probes different proportional depths depending on particle size. Electrospray ionization mass spectrometry (ESI-MS) has also been used to study aerosol processes since the ionization source produces droplets from the analyte/reactant solution before mass analysis.[47] For instance, this technique was used to show that the aerosol surface resisted proton transfer compared to the bulk unless ionic species were present.[17] ESI-MS also demonstrated that common carboxylic acid species were more acidic at the droplet surface than in the bulk. Time-of-flight mass spectrometry (ToF-MS) was used to analyze the surface oxidation of organics on laboratory generated aerosol particles in real time and showed accelerated oxidation rates on core-shell particles as opposed to pure particles. Even though surface enhancement was observed, this technique is not surface-selective. These MS-based techniques have provided much information about droplet systems as they exist in the air, but their use has been cautioned, specifically ESI-MS, as the multiphase nature of the particle generation process complicates reaction systems and may in itself contribute to chemical reaction acceleration.[47] An adaptation of MS which allows pseudo-surface probing is easy ambient sonic-spray ionization MS (EASI-MS), which has been shown to probe a certain depth at the surface of solid core-shell aerosol particles. This method is not inherently surface-sensitive and instead must be tuned to probe a certain interfacial depth. Nevertheless, these *in-situ* methods are not surface-selective and can sometimes introduce new variables to complicate aerosol surface studies. Due to information gaps caused by the lack of *in situ* analyses and interfacial specificity, we now shift our focus to nonlinear optical spectroscopic techniques, which solve both of these problems.

With an introduction to nano-droplet and micro-droplet surface properties outlined, we believe that it a summary of outstanding topics regarding the different applications for them is appropriate. Although ultrasonic phase-shifting nano-droplets have shown preliminary promise in extravascular therapy and imaging applications, such treatments still hold safety concerns. For instance, negative effects have been noted in animal studies due to the rapid changes in pressure associated with the vaporizing droplet, and these treatments have not yet advanced to the stage of clinical trials. Partial solvation at droplet surfaces has been proposed as a leading cause for accelerated reaction rates in sprayed and suspended systems, along with reactant concentration leading to concentration gradients.[7] Although the droplet surface is generally ascribed to cause such accelerations, analyses into reaction mechanisms often infer mechanisms based on non-surface selective methods. The surfaces of atmospheric aerosol droplets is continuously relevant to atmospheric chemistry and climate science.[11] However, modern developments in our understanding of aerosol surface reactions and uptake stems from computations and studying

planar analogs. The models developed from these studies may also benefit from experiments which can directly observe such processes with interfacial sensitivity. Due to information gaps caused by the lack of *in situ* analyses and interfacial specificity, we now shift our focus to nonlinear optical spectroscopic techniques, which may solve both of these problems.

Second-Order Nonlinear Optical Scattering

To understand the breadth of attempts and the difficulty of using nonlinear optical spectroscopy to probe droplet surfaces in air, we think that it is necessary to start from its origin and outline the progress made over the last several decades. After providing a brief background on second-harmonic generation (SHG) and sum-frequency generation (SFG) spectroscopies from planar surfaces, we will discuss the development of second-harmonic scattering (SHS) and vibrational sum-frequency scattering (VSFS) experiments, as well as the theoretical works which laid the foundation for the modern nonlinear optical scattering spectroscopy field. We will then give brief background on the mechanism of SF spectroscopy, and for the adsorption of molecules to planar and droplet surfaces from within and without.

SHG and SFG are second-order nonlinear optical techniques which are forbidden from bulk systems with inversion symmetry which makes them sensitive to interfaces and surfaces.[26, 48] The first experimental demonstration of the surface-specificity of SHG date back to the mid 1960's.[49, 50] After its success, the first interfacial vibrational spectrum from VSFG was reported by Shen et al. in 1987.[51] These developments opened up a world of possibilities for nonlinear optical interfacial spectroscopies.[52-56] Even though SHG and SFG have had an immense impact on understanding the physical and chemical properties of diverse planar interfaces, we now consider how the techniques can be and have been applied to curved droplet surfaces, such as those in emulsions and aerosol droplets.

Nonlinear Optical Scattering in Dispersive Media

Wang et al first demonstrated interfacial SHS from a suspension of centrosymmetric nanospheres in an aqueous medium.[57] It was found that for such a system, if the distance between opposingly oriented molecules is on the order of the excitation wavelength, the signals from two such species are not cancelled and the SHS signal can propagate, *i.e.*, particle diameter ~λ. This breakthrough work used an aqueous malachite green (MG) solution, a nonlinear chromophore, and polystyrene latex (PSL) nanospheres 1 μm in diameter. The nonlinear dependence of the SH signal on MG bulk concentration showed that the signal was in fact from molecules adsorbing onto the surface of the spheres. The authors further defended that the observed signal was coherent SHS through the linear dependence of signal intensity with particle density. This pioneering work offered the vast toolbox of nonlinear optics to the very relevant fields of colloids, nano- and micro-droplets, and aerosol particles. Shortly after demonstrating the capability of SHS, they extended the method to sub-micron oil droplet surfaces in aqueous emulsions. They not only showed the ability to extract surface adsorption densities and free energies,[58] but also determine surface charge densities and electrostatic potentials through SHS experiments. It did not take long before this novel technique was adopted by other researchers to study the adsorption properties of molecules onto surfaces in colloidal systems.[59, 60] Using MG and 1 μm diameter PSL microspheres, Dai et al used a liquid-jet SHS setup and a digital titrator to monitor the adsorption of MG on PSL surfaces in real time.[61] A Langmuir adsorption model was used and allowed the authors to determine surface coverage and adsorption free energy values for the system. By using this same titration method,

the authors observed the adsorption of surfactant molecules onto the PSL microspheres. As the surfactant molecules displaced MG molecules, the SHS signal decreased accordingly, and isotherms were conducted, allowing calculations of surface coverage and adsorption free energy for the surfactant to be calculated as well. The use of a femtosecond pulse laser with high repetition rate, commonplace for SHS experiments, results in low pulse energy and therefore minimal sample damage. This feature allows SHS to be applied to fragile systems like liposomes. For example, Eisenthal et al showed in 1998 that SHS could be used to measure the transport kinetics *in situ* of MG across a liposome bilayer.[62] Impressively, this property was later exploited to allow the use of SHS to probe transport kinetics, label-free, in real time across cell membranes some years later,[63] thoroughly planting a foothold for nonlinear optical scattering in biological sciences. More recently, SHS was used to probe the orientation of water molecules at water droplet surface in an emulsion.[64] This work observed the shifts in hydrogen bonding for water nano-droplets as micelles formed around them with increasing surfactant concentration. Nevertheless, second-harmonic generation only provides electronic molecular information, often requires the use of second-harmonic active dyes, and cannot identify molecular functional groups at interfaces like VSFG can.[65]

Sum-frequency scattering from a colloidal suspension was originally reported in 1998 by Wang et al. who used two nondegenerate visible pulses to observe the interfacial signal at the sum frequency.[58] The next step was to apply the process with a vibrationally resonant IR pulse and a visible upconverting pulse, as was done by Bonn et al. in 2003.[66] This report displayed VSFS spectra at four polarization combinations, drew orientational information from spectral features, mapped the measured radial scattering pattern from the experiments, and applied the Rayleigh-Gans-Debye (RGD) scattering theory to the results. This novel demonstration introduced molecular identification at particle surfaces to the fields of physics, chemistry, engineering, biology, and many others. Using submicron hexadecane droplets in an aqueous emulsion, Roke et al used VSFS to show that the effect on surface tension by the surfactant SDS is drastically reduced for nano-droplet systems versus planar systems.[67] Another interesting application of VSFS was its use to monitor phase changes of both oil and water species in freezing emulsions.[68] The Richmond group has made significant strides in sum frequency generation spectroscopy and has more recently used the method to study colloidal systems. For example, they investigated the effects of absorptive solvents in emulsion systems for isotopic water and the impact of the cuvette path length on absorption of incident IR radiation. [69] This work found that cuvettes with path lengths of no more than 50 μm should be employed and demonstrated that spectral corrections could be performed on affected VSFS signals, even though decreased signal intensities were apparent. The effects of the introduction of NaCl to the aqueous phase of oil-in-water emulsions have also been investigated using VSFS, comparing the system to the planar oil/water interface.[70] It was found that the addition of salt greatly increased the adsorption of nonlinear ionic surfactants to the droplet surface and concluded that the effect of salt in the aqueous phase greatly depends on the structure of the surfactant employed. This work provided valuable information because surfactants are often used to stabilize emulsions in such cases. This group has also used VSFS to confirm that the negative charge of pH-switchable surfactants increases droplet stabilization in oil-in-water emulsions while the neutral species destabilizes the system. [71] VSFS has also been extended into biologically motivated uses, where it was recently used to study proteins at the surface of nano-droplets in an emulsion.[72] Not only was VSFS used in this case to observe the orientation of the proteins at the droplet surfaces, but it was found that the protein orientation therein was different

than at the flat surfaces. This finding could have major implications as nanoparticles and droplets are finding more and more usefulness in biology and medicine. Recently, VSFS has demonstrated ability to identify peptide species at nano-droplet surfaces as well as their orientations *in situ* under ambient conditions.[72] As can be expected with the experimental developments for second-harmonic and sum-frequency scattering came theoretical models for the novel techniques.

Following the first experimental demonstration of SHS from micrometer-sized centrosymmetric spherical surfaces, a theoretical model based on the excitation of nonlocal electronic dipoles and local electronic quadrupoles with an emphasis on the spherical particles being small compared to the incident wavelength was developed.[73] This work laid the footing for the improvement of SHS experiments in the future in terms of both efficiency and what knowledge might be gained. RGD scattering theory was applied to SHS experiments using micron-sized particles suspended in liquid in 2001, and aligned experimental and theoretical findings in a straightforward manner.[74] These angle-dependent experiments revealed an anisotropic scattering pattern for the SH light, distinct from that of linearly scattered light from the same system as well as SH light generated in bulk media. RGD scattering theory was first applied to SFS data in 2003, revealing the local second-order surface susceptibility as well as effective nonlinear susceptibility per irradiated spherical particle.[66] An extension of the SFS theory using a more general Mie scattering theory was performed in 2009, wherein the application of index of refraction mismatching resulted in new developments in the computed SF scattering pattern.[75] The RGD scattering theory was applied to SHS and SFS experiments again in 2010 for particles suspended in water, demonstrating a method for determining the orientational angle of functional groups at spherical surfaces.[76] This work used the intensity ratios of scattered signals with different polarization combinations to calculate molecular orientation at the spherical surface. Interestingly, the polarization intensity ratios recently observed by Qian et al from VSFS experiments from aerosol droplets in air were directly opposed to the proposed theoretical values. These differences are outside of the scope of this article as this issue has not yet been fully resolved. We refer the interested reader to the original works and following comments.[77-79] A possible issue with the proposed theory is that it does not account for Rayleigh-scattered (diameter < λ) nonlinear signals while also accounting for the differences in the refractive indices of the surrounding medium, the medium/particle interface, and the suspended particle, as the inclusion of refractive indices impacted scattering patterns previously.[75]

Basic Principle of SHS and SFS.

SFS is a process by which two incident photons, one higher energy upconverting pulse usually in the visible or near-IR range (ω_1), and the other in the near to mid IR which is resonant with an electronic or vibrational mode of the analyte species (ω_2). The two incident photons are annihilated to generate a third photon whose frequency is the sum of the two incident frequencies(ω_{SF}):

$$\omega_{SF} = \omega_1 + \omega_2. \quad (1)$$

SHS, for the purposes of this article, can be viewed as the special case of SFS where $\omega_1 = \omega_2$ such that $\omega = 2\omega_1$. For a SFS process, the intensity of ω can be described by[80]

$$I(\omega_{\mathrm{SF}}) \propto E(\omega_{\mathrm{SF}})^2 \propto \left|\chi_{eff}^{(2)}\right|^2 I(\omega_1) I(\omega_2), \tag{2}$$

where $I(\omega_j)$ is the intensity of the j beam, $E(\omega_{\mathrm{SF}})$ is the electric field of $I(\omega_{\mathrm{SF}})$, and $\chi_{eff}^{(2)}$ is the second-order nonlinear susceptibility which describes the macroscopic response of the irradiated sample to the incident radiation. The susceptibility is related to the surface number density, N_s, by[80]

$$\chi_{ijk}^{(2)} = N_s \sum_{i'j'k'} \langle R_{ii'} R_{jj'} R_{kk'} \rangle \beta_{i'j'k'}^{(2)}, \tag{3}$$

where $\beta_{i'j'k'}^{(2)}$ is the molecular hyperpolarizability which describes the molecular second-order characteristics, and R_{ijk} are the components for the transformation matrix from the molecular coordinate system to the macroscopic laboratory coordinate system.[80]

For a suspension of spherical particles with centrosymmetric bulk composition in an arbitrary medium, the electric field of the sum-frequency signal, $E(\omega)$, can be expressed as[81]

$$\vec{E}(\omega_{\mathrm{SF}}) = \frac{K_1^2 e^{K_1 r}}{\varepsilon_1(\omega_{\mathrm{SF}}) r} \left(\hat{K} \times \vec{P}_{eff}\right) \times \hat{K}, \tag{4}$$

where $K_1 = \sqrt{\varepsilon_1(\omega_{\mathrm{SF}})} K$, $\varepsilon_1(\omega_{\mathrm{SF}})$ is the dielectric constant of the scattered SF electric field in the surrounding medium, K is the wavevector of the scattered SF electric field in vacuum, r is the radius of the particle, and $\hat{K}$ is the direction of the scattered SF field. Additionally, the effective SF polarization is proportional to the second-order nonlinear susceptibility:

$$\vec{P}_{eff} \propto \chi_{eff}^{(2)}. \tag{5}$$

The polarization term contains both interfacial and bulk contributions to the signal, as well as $\chi^{(3)}$, the third-order susceptibility, which is related to surface charge and electric field-induced SHS discussed later.

Experimentally, the observed the radiated power per unit solid angle of the SF signal, $dP(\omega_{\mathrm{SF}})/d\Omega$, detected through an analyzer allowing polarization state $\hat{e}$ can be described by

$$\frac{dP(\omega_{\mathrm{SF}})}{d\Omega} = \frac{c r^2 \sqrt{\varepsilon_1(\omega_{\mathrm{SF}})} \left|\hat{e} \cdot \vec{E}(\omega_{\mathrm{SF}})\right|^2}{2\pi}, \tag{6}$$

where c is the speed of light in vacuum.

An important parameter which is relevant to SHS, ESFS, and VSFS is resonance between the incident or generated light with an electrical or vibrational transition in a probe molecule. For VSFS, the incident IR pulse is resonant with a vibrational mode of the analyte. However, for SHS and ESFS, the generated signal is resonant with an electronic transition of the analyte. This is important in experimental implementations because the electronic resonance enhances the generated signal, and it is so called "resonance enhanced." Resonance enhancement is demonstrated below in SHS experiments where probe molecules were paired with incident

wavelengths: DiA4 has an electronic transition at 475 nm and was thus paired with an 800 nm incident light to give the resonance-enhanced SHS signal at 400 nm,[82] and later with a 1030 nm incident light to give the resonance-enhanced SHS signal at 515 nm.[83] Later SHS paired the 1030 nm incident light with crystal violet, which has an absorption maximum at 586 nm,[84] resulting in the resonance-enhanced signal at 515 nm.[83] Lastly, the ESFS spectrum of malachite green was observed at 613 nm, nearly coincident with the molecule's absorption maximum at 618 nm.[85] Such resonances are essential when designing nonlinear scattering experiments to increase success.

Experimental Challenges in Second-Order Nonlinear Scattering

A fundamental difference between SHS and SFS in air versus in an emulsion or from a planar surface comes from the lack of density in the sample. Consider, for example, a cloud of aerosol droplets with a density of 10^6 cm^{-3}, with all the droplets having a diameter of 100 nm. For an incident 3.5 μm laser focused to a spot with 100 μm diameter, about 18 of the particles will be within the Rayleigh length, the contributing region, of the laser. Next, assume that each droplet has a monolayer of coverage of an ideal molecule with a density of 2×10^{14} cm^{-2}.[21] This then gives about 6.3×10^4 molecules per particle and 1.1×10^6molecules irradiated to produce the scattering signal, assuming that all molecules on all irradiated particles contribute equally. Now, let us consider the same laser conditions, but instead consider an emulsion in D_2O of 100 nm diameter particles with a density of 10^{12} cm^{-3} in a sample cell with 1 mm length.[79] Such an arrangement will give about 5×10^{11} molecules irradiated to produce the scattering signal. This does not consider the absorption of incident light by the medium which can be over a majority depending on path length.[69] Lastly, let us consider the planar liquid surface with a monolayer of coverage as before. For such a system, there are 1.6×10^{10} molecules irradiated to produce the second-order signal from the planar surface. Another key factor in the difficulties associated with second-order scattering from droplets in the air is the amount of collected signal. Assuming that little light is absorbed by the airborne droplets or the surrounding air, still only about 60° of the assumed 360° scattered light is collected, whereas nearly all generated light can be collected for the planar system. For scattering experiments in dispersive media, 5×10^5 more molecules are available, and about10^4 more are available in planar experiments.

Further experimental difficulties and theoretical concerns arise in the real-world scenario of nonlinear scattering from droplets in air: available aerosol generators for particles ~100 nm in diameter produce a cloud of polydisperse droplets with lognormal size distribution and concentrations limited to around 10^7 cm^{-3}. Such particle densities result in the weak signal from aerosol droplets in scattering experiments, which can be improved by increased incident laser energy and collection efficiency. The polydispersity of the aerosol cloud results in variable available surface area for adsorption of analytes and nonlinear signal generation, as well as mixed light scattering properties based on particle diameter. To simplify the extension of theory to these experiments, both size-dependent and scattering angle-resolved experiments are required. However, droplet and particle classifiers which filter particles based on size have very poor efficiency which does not bode well for the already weak scattered signal. Furthermore, angle-resolved experiments will dramatically reduce the amount of generated signal which enters the detection system and likewise reduce the observable signal. Interactions between particles can also complicate the explanations of experimental results. For the aerosol cloud described above, a simple calculation gives that the distance between two particles is about 100 μm. On the other hand, an emulsion with 10^6 times greater density results in particle spacing of about 0.9 μm. As such, inter-particle interactions cannot be ignored in the case of an emulsion. Additionally, a

system of polydisperse particles will complicate considerations of particle-particle interactions, furthering the need for size-dependent nonlinear scattering experiments. Describing such interactions is outside the scope of this article. We note that the rough calculations given here do not consider the many intricacies associated with these experiments such as incident fluence, hyperpolarizabilities, etc., but hope to give the reader some perspective on the troubles associated with the task.

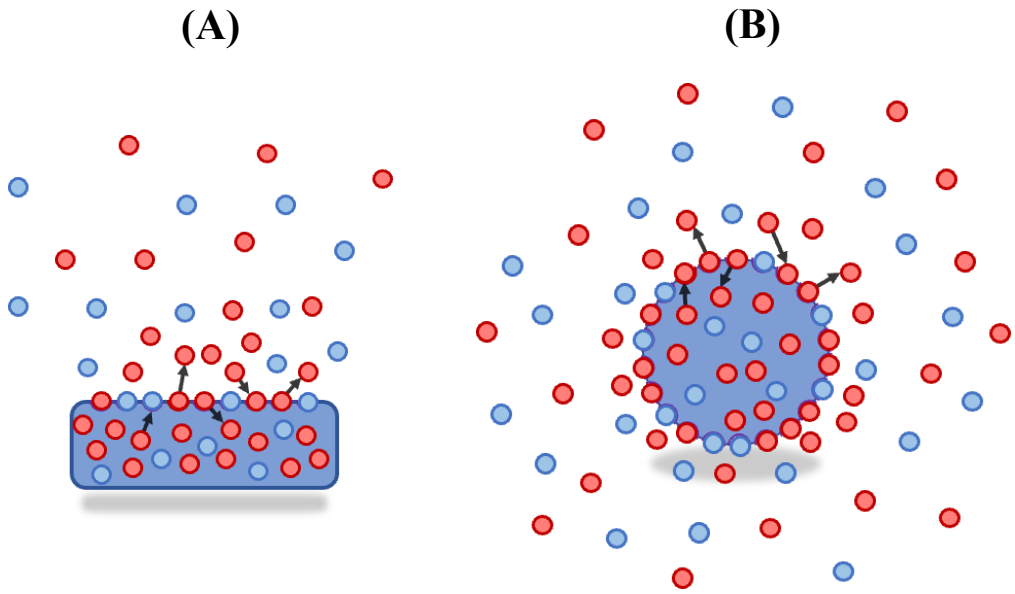

Figure 3. Adsorption and desorption of species at planar (A) and droplet (B) surfaces from within the bulk and the gas phase.

Surface Adsorption of Droplets.

Adsorption of molecules to droplet surfaces can happen from within, bulk-to-surface, or from the outside, gas-to-surface. Interfacial uptake is the process of gas phase species outside of a droplet being taken into its bulk through the gas/droplet interface.[8] In this case we do not consider chemical reactions occurring along the way. This process is crucial as it dictates bulk phase reactions with external species and is governed by the gas/droplet interface. The first step involves the adsorption of the gas phase species to the droplet surface, where it can either desorb back to the gas or be taken into the bulk of the droplet.[86] At the gas/droplet interface, the adsorbate is in a thermodynamic well, where it will either need to overcome an energy barrier for desorption back to the gas phase or a higher barrier to be taken into the bulk. To complete the uptake process, the adsorbate must overcome the barrier to be taken into the bulk via solvation at the interface: a critical cluster size (dependent on the adsorbate) necessarily solvates the adsorbate molecule and completes the uptake process. Uptake processes, reactive or otherwise, can have a significant

impact on aerosol properties including lifetime, hygroscopicity, organic reactivity, and optical properties.[87] Although uptake is a cornerstone of aerosol chemistry, it is not in the scope of this feature. The remainder of this article focusses specifically on the process of interfacial adsorption for both gas-to-surface and bulk-to-surface processes.

When studying matters of surface coverage and adorption, either the planar surface of a bulk solution or the tightly curved surface of a droplet, the Langmuir adsorption model is important to consider. Even though we are primarily concerned with adsorption at the gas/aerosol droplet interface, we must first consider the simplest and original cases. The original Langmuir adsorption model described the kinetics of an ideal gas adsorbing onto a solid surface with a finite number of identiccal adsorption sites. Specifically, the process considered both adsorption and desorption of the adsorbate in question and was described as follows: First, the rate of adsorption of an incident gas species, r_{ads}, is proportional to the pressure of the gas at a constant temperature. Second, r_{ads} depends on both the probability of adsorption, p_{ads}, (instead of reflection) when the gas impacts an empty adsorption site. Lastly, the rate of desorption is equal to the rate of desorption at maximum surface coverage, $r_{des,max}$, multiplied by the fraction of occupied adsorption sites, θ.[88] Assuming that adsorbates do not interact with each other in bulk or adsorbed states, the process of adsorbates (M) filling empty sites (ES) to give filled sites (FS) is described by the equilibrium

$$\mathrm{M} + \mathrm{ES} \underset{k_{-1}}{\overset{k_1}{\rightleftharpoons}} \mathrm{FS}, \tag{7}$$

where k_1 and k_{-1} are the adsorption and desorption rate constants, resepctively, and [88]

$$\theta = \frac{r_{ads}p_{ads}}{r_{des,max}+r_{ads}p_{ads}} = \frac{KP}{1+KP} = \frac{N_s}{N_{max}}, \tag{8}$$

where K is the Langmuir constant, Ns is the number of adsorbed species (FS), and N_{max} is the number of possible adsorbtion sites (ES +FS), both per unit volume. This model was based on previous indirect observations of gases adsorbing onto the inside of a glass lightbulb, but was later quantified with the adsorption of nitrogen gas on muscovite which aligned well with the simple model above. Over the last century, as experimental techniques and physical understandings grew, this model has been expanded to more complex adsorption systems, such as surfaces with continuously different adsorption affinities and multi-layer adsorption models.[88] However, only the considerations from the simplest model are necessary in this article, as we now shift our focus to liquid surfaces and the air/water interface.

For an aqueous system, the change in solute species adsorbed to the air/water interface over time is given by [89]

$$\frac{\mathrm{d}N_S}{\mathrm{d}t} = k_1 \frac{C}{55.5}(N_{max} - N_s) - k_{-1}N_s, \tag{9}$$

where C is the molar concentration of M in the solution and 55.5 is the molar concentration of water. This will be referred to as the Langmuir model from now on. Now, if we consider when the system is at equilibrium: $\mathrm{d}N_s/\mathrm{d}t = 0$, and Eq. 9 can take the form of [89]

$$\frac{N_s}{N_{max}} = \frac{C}{C+a}, \tag{10}$$

where

$$a = 55.5b, \text{and } b = \frac{k_{-1}}{k_1} = e^{\frac{\Delta G_{ads}}{RT}}. \tag{11}$$

This shows the direct relationship between the fractional surface concentration and the free energy of adsorption, ΔG_{ads}. Although this was by no means of the first application of Langmuir's adsorption theory to solute adsorption to the solution surface, this specific use of the model was used to explain experimental trends in SHG experiments. Early applications of this model sought to form a linear relationship with experimental data and the adsorption process. It was found, in fact, that N_s is proportional to the SH electric field, E_{SH}, and that $1/N_s$ is proportional to $1/C$. This relationship provided a slope-intercept type relationship of [89]

$$\frac{1}{N_s} = \frac{a}{N_{max}}\frac{1}{C} + \frac{1}{N_{max}}. \tag{12}$$

This formulation provides determination of ΔG from experimental data, where it is part of the slope of the line made by Eq. 12. Working instead with N_s, we can achieve[89]

$$N_s = \frac{CN_{max}}{C+ab}. \tag{13}$$

This method of relating the SHG/SFG electric field to the surface number density does, however, seem unnecessarily convoluted. Starting with Eq. 9, Equilibrium gives that $\mathrm{d}N_s/\mathrm{d}t = 0$, and by setting K as k_1/k_{-1}, we get the simpler relation data [58, 80]

$$E_{SH,SF} \propto \frac{N_s}{N_{max}} = \frac{KC}{KC+55.5}, \tag{14}$$

which can be used for both second-harmonic and sum-frequency experiments and has shown good fitments to experimental data. The models described thus far have been shown to be efficient for descriptions of solute activity at the air/water interface as well as adsorbing gas therein. However, this model may not be well suited for systems with significantly more surface area like droplets. For more details which consider dynamic and kinetic models of adsorption and desorption in more complex systems, we refer the reader to more pointed literature. [88]

Shifting the focus of adsorption at a planar surface to that at a spherical surface should not require much adaptation; after all, the central difference is geometry. However, this simplification likely will depend on the details of the system containing curved surfaces. A simplification occurs when deriving the rate equation in the Langmuir system, namely, the assumption that $N_s << C$, without which would result in Equation 6 taking the form of [58]

$$\frac{\mathrm{d}N_s}{\mathrm{d}t} = k_1\frac{C-N_s}{55.5}(N_{max} - N_s) - k_{-1}N_s. \tag{15}$$

This simplification is reasonable when considering a bulk system with a single, planar surface which is much smaller than its total volume. However, if we consider an oil in water emulsion, a suspension of particles in an aqueous solution, or airborne droplets, it is easy to imagine a system in which over half of the total volume lacks the solute. In this case, the surfaces of these spheres provide significant interfacial area, much greater than the surface of a bulk solution. With the simplification no longer holding, the fractional surface coverage now becomes[58]

$$\frac{N_S}{N_{max}} = \frac{(C+N_{max}+55.5/K)-\sqrt{(C+N_{max}+55.5/K)^2-4CN_{max}}}{2N_{max}}. \quad (16)$$

With the consideration of increased surface area to volume ratio for emulsions and particle suspensions, this model was shown to fit well to experimental adsorption data for these systems. This model also allows the quantification of N_s, not just ΔG, since N_{max} can now be extracted from the isotherm fitting parameters. This formulation of the Langmuir adsorption might also be applicable when considering adsorption to a droplet surface from within its bulk medium. As discussed previously, the size of a droplet can significantly affect the availability of solute species to adsorb to its surface. Now that we have covered sufficient history and principles relevant to droplet systems, and the uniqueness of the droplet surface, we now describe the recent developments in surface-specific observations of droplets in the air from nonlinear scattering.

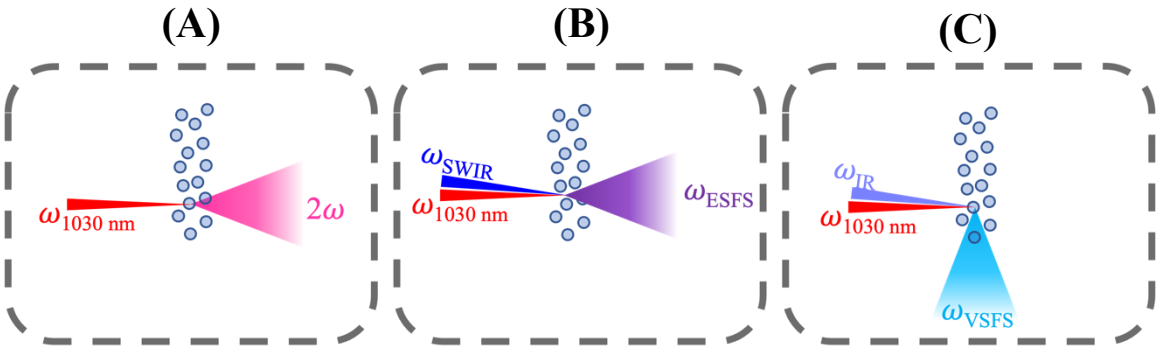

Figure 4. A schematic of second-order scatterings techniques for laboratory-generated droplets in air, including SHS (A), ESFS (B), and VSFS (C).

Second-Order Nonlinear Optical Scattering from Droplets in Air

Experimental Conditions for Second-Order Scattering from Droplets in Air.

This section outlines the experiments for SHS,[82, 83, 90] ESFS,[85] and VSFS[77, 78, 91] from droplets in the air, as well as the difficulty of the experiments which arises from using droplets in air instead of in an emulsion or a planar surface. Additional details can be found in the literature.[77, 78, 82, 83, 85, 90]

Generation of Aerosol Droplets. In the examples of SHS, ESFS, and VSFS from aerosol droplet surfaces, an aerosol generator was used. Using N_2 gas, the aerosol generator drew from a stock solution of NaCl for its environmental relevance. Different concentrations of salt in the stock solution can affect the size distribution of the generated droplets. For example, solutions of 0.5

and 1.0 M NaCl, the average droplet diameters were 40 and 100 nm, respectively, with a density of 10^6-10^7 cm^{-3}.[78, 82] The stream of aerosol droplets was directed to the plane of incidence for nonlinear scattering experiments and was collected by a catch vessel connected to a vacuum pump.

Second-Harmonic Scattering. Two example SHS setups have been reported for aerosol surfaces: one using an 800 nm femtosecond (fs) laser [82] and the other using a 1030 nm fs laser [83, 90]. The 800 nm system operated at a repetition rate of 80 MHz with a peak power of 10.6 GW cm^{-2} at the aerosol sample. The 1030 nm system had a tunable repetition rate up to 1 MHz with peak energy of 65 GW cm^{-2} at the sample. For both setups, the generated SHS signals were collected in the forward (0°) propagation direction and focused into spectrometers fitted with either a photomultiplier tube (PMT) and single photon counter (SPC), or a charge coupled device (CCD) detector; both of which are sufficient. The 1030 nm system presented meaningful advantages over the original 800 nm SHS system: it offered complete tunability of repetition rate to maximize collection efficiency. Tunability of repetition rate can increase the SHS signal since its intensity is proportional to both incident energy and power (which increases with repetition rate). The implementation of the CCD detector in the later system dramatically increased experimental collection efficiency by collecting the entire emission spectrum at once instead of relying on tuning a spectrometer to produce a spectrum using the PMT on the earlier SHS system. These differences and improvements on the SHS experimental setup are discussed in a later section.

Electronic Sum-Frequency Scattering. The same 1030 nm fs laser from later SHS experiments was also used as the powerhouse for ESFS experiments. An optical parametric amplifier (OPA) was used to generate a tunable fs shortwave IR (SWIR) pulse, while the fs 1030 nm pulse was converted to ps using a pulse shaper. Operating at 100 kHz, the 1030 nm and SWIR pulses had peak powers of 79.5 and 397 GW cm^{-2} at the sample, respectively. The temporal overlap of the two incident pulses was regulated, as were the polarizations of incident and signal beams. Lastly, the ESFS signal was collected in the forward direction with a total collection angle of 60° before being focused into a spectrometer fitted with a CCD detector.[85]

Vibrational Sum-Frequency Scattering. The same 1030 nm fs laser-amplifier system was used as the light source for VSFS as well. In this case, an OPA was used to generate the fs mid-IR pulse and the picosecond (ps) 1030 nm pulse was achieved with an etalon. Upon overlap at the aerosol stream, the 1030 nm and IR pulses had peak power values of 106 and 224 GW cm^{-2}, respectively. Again, the polarizations of the incident and generated signals were tunable. The generated VSFS signals were collected at 90° relative to the propagation of the incident 1030 nm beam. After its previous success in SHS and ESFS, a spectrometer fitted with a CCD was used to collect the VSFS spectral signals.[77, 78]

Recent Progress in Second-Order Scattering from Droplets in Air.

In situ surface specific observations of droplets in air may fill in the gaps left by *ex-situ*, destructive, or non-interface specific methods. One of the most relevant applications of such a technique is to atmospheric science and chemistry, as the chemical and physical properties of the aerosol surface are crucial to atmospheric processes and cannot be approximated effectively.[8, 11, 36, 92, 93] The very small radius of curvature of aerosol surfaces makes their analogy to the planar air/liquid interface convoluted. Furthermore, replacing the surrounding medium with a liquid in

which particles or droplets are suspended results in extensive particle/medium interactions, inefficient transmitted signal collection and different scattering patterns. In this section, we discuss the development and recent progressions in second-order scattering techniques for droplet surfaces in air.

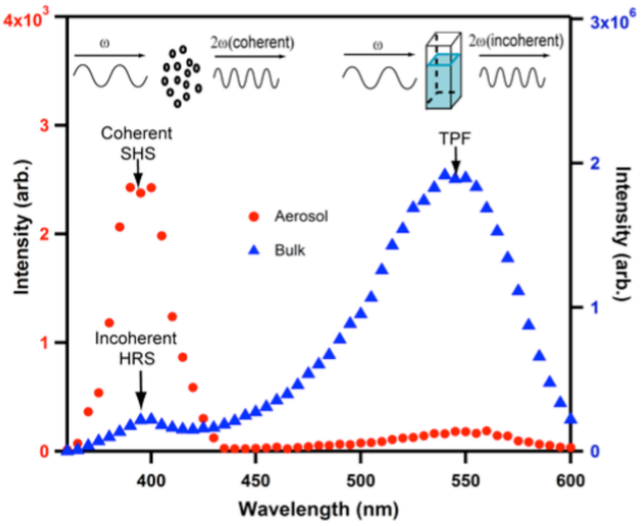

Figure 5. Two-photon emission spectra from droplet (red circle, left axis) and bulk solution (blue triangle, right axis) samples from the same stock solution of DiA-4 in 1.0 M NaCl under 800 nm excitation.
Reprinted with permission from Ref. 82. Copyright 2016 American Chemical Society.

Second-harmonic scattering (SHS) from droplet surfaces in air.

SHS from droplet surfaces in air was first demonstrated in 2016.[82] This observation of organics at droplet surfaces was achieved using an aerosol generator which drew from a seed solution of 1.0 M NaCl containing 20 μM trans-4- [4-(dibutylamino)styryl]-1-methylpyridinium iodide (DiA4), an SHG-active nonlinear chromophore, using a constant stream of N_2 gas to produce droplets with a density of ca. 10^7 cm^{-3} and an average diameter of 100 nm. The droplets flowed into a sealed chamber which was maintained at 100% relative humidity to ensure that they stayed aqueous and did not crystallize. Using a high repetition rate femtosecond laser with a central wavelength of 800 nm, a strong peak was observed at 400 nm: resonance-enhanced SHS, which was not observed when using droplets produced form the NaCl solution only. DiA4 was used in this experiment due to its high hyperpolarizability. Many SHG-active chromophores were tested using this system before DiA4, none of which provided an observable signal. For this system, the SH signal form DiA4 was resonance-enhanced due to the absorption peak of the molecule at 475 nm from the $S_0 \rightarrow S_1$ transition. To provide evidence that the SHS signal was mainly from the droplet surfaces, an equimolar amount of the surfactant CTAB was added to the stock solution and the peak at 400 nm decreased by over half as the highly surface-active CTAB displaced the DiA4 molecules. The SHS signal was not the only observable process near the second-harmonic of the incident 800 nm probe; in fact, it was not the only process that has an emission at 400 nm. For the bulk solution of 20 μM DiA4, the emission spectrum showed two peaks: hyper-Rayleigh scattering (HRS) at 400 nm and two-photon fluorescence near 550 nm, as shown in Figure 5 (blue triangles). HRS is an incoherent process which gives a signal at the second-harmonic of an incident laser and TPF is molecular fluorescence which is induced by two-photon excitation. Both processes are

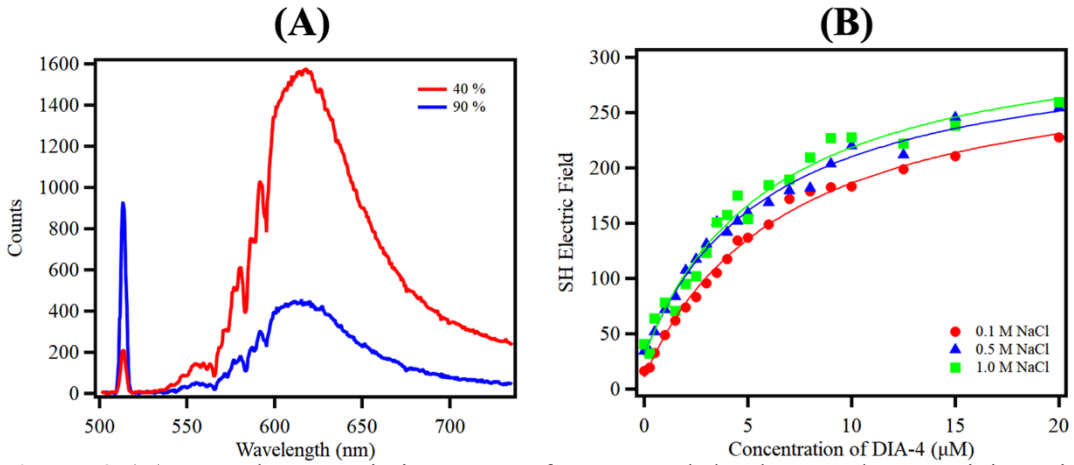

Figure 6. (A) Two-photon emission spectra from aerosol droplet samples containing DiA-4 under 40% (red) and 90% (blue) relative humidities. (B) SHS electric field versus stock DiA-4 concentration for stock salt concentrations of 0.1 (red circle), 0.5 (blue triangle), and 1.0 M (green square).
Reprinted with permission from Ref. 90. Copyright 2019 American Chemical Society.

bulk-dominated systems but their potential effect on the SHS signal had to be investigated. Accordingly, the emission spectra of both the bulk solution and aerosol particles generated from the same solution when irradiated with 800 nm light are compared in Figure 5. The 400 nm peak from the bulk solution was not SHG because the random orientation in the bulk results in the cancellation of such coherent photons. On the other hand, DiA4 molecules on the particle surfaces have a similar orientation, resulting in the additive increase of the SHS signal. Both TPF and HRS signals are highly dependent on bulk DiA4 concentration and are expected to retain the same intensity ratios. The emission spectrum from the aerosol sample (red circles) displays an intense peak at 400 nm and a much weaker one near 550 nm: SHS and TPF, respectively. The TPF signal from the aerosols containing DiA4 was much weaker due to much fewer molecules being illuminated at once in the sample. As such, the HRS contributions to the signal at 400 were deemed to be negligible, again due to the much smaller sample volume. Finally, this report compares the two-photon emission intensities of the SHS and HRS signals at 400 nm for both droplet and bulk samples from the same stock solution for DiA-4 concentrations from 0 to 25 μM. As an incoherent bulk process, the HRS intensity for the liquid sample obeys Beer's law and increases linearly with DiA4 concentration. On the other hand, the SHS signal increases with a nonlinear Langmuir type trend with increasing DiA4 concentration as SHS is a coherent surface specific process. This pioneering work demonstrated that nonlinear optical scattering was possible form particles suspended in air, breaking through a wall that was hit by the nonlinear optical community after over a decade. Now that SHS from droplet surfaces had been demonstrated, it was necessary to optimize the system to increase experimental efficiency to make the novel technique more accessible.

The next step in the development of second-order scattering from droplet surfaces was to uncover and employ an optimal experimental system.[83] A 1030 nm fs laser system with either 10 W at single shot to 1 MHz repetition rate, or 1 W at 80 MHz was used as the light source for the experiments. Spectral collection was completed by a spectrometer fitted with both a CCD and PMT/SPC for efficiency comparisons. The same aerosol generation method as used in Wu et al

2016 was applied, with 1.0 M NaCl seed solution and 20 μM crystal violet (CV). Although CV a smaller hyperpolarizability than DiA4[82] which would decrease its SHS signal, CV has an absorption maximum at 586 nm,[84] producing the resonance-enhanced SHS signal at 515 nm. The two-photon emission spectra were compared for both droplet and bulk samples of the same solution of 20 μM CV in 1.0 M NaCl. The spectrum for the bulk sample showed a weak peak at 515 nm, incoherent HRS, and an intense band at 670 nm attributed to TPF that was five times more intense than the corresponding HRS. For the droplet sample, the peak at 515 nm, SHS, was 21 times stronger than its TPF, and the TPF produced a spectrum with peaks at 620, 725, and 830 nm, suggesting that the droplet environment was localized and produced little spectral broadening. Again, the TPF is much smaller than the SHS due to the low sample volume in the droplets and therefore fewer CV molecules being probed. With the peak intensity ratios remaining constant for HRS and TPF, the SHS signal would be over 100 times stronger than the HRS contributions, rendering them negligible. Comparing the intensities for the SHS and TPF signals from the droplet sample at different CV concentrations showed a Langmuir-type signal increase for SHS and a linear increase for TPF with increasing CV concentration, confirming that the SHS signal came from the nano-droplet surface and the TPF was from the underlying bulk. The next steps in this report analysand ways in which SHS experiments could be made easier and more efficient. Since the SHS signal intensity is proportional to the incident pulse energy and average power, one might conclude that a higher-powered laser system would increase the SHS intensity. However, it was found that pulse energies exceeding 1 μJ resulted in white light generation from the droplet sample, making the SH signal undetectable. The authors concluded that although they achieved the best results with 1 μJ at 1 MHz. This is because the SHS signal intensity is proportional to both incident energy and power. Since higher energy incident pulses induced higher-order nonlinear responses, the increase in repetition rate over 100 kHz also increased the SHS signal. It was also noted that others may find success with different settings due to the inevitable tradeoff between pulse energy, average power, and repetition rate for laser systems. It was also found that the CCD detector and PMT/SPC gave similar signal-to-noise ratios (SNR) at different laser repetition rates, and both have excellent quantum efficiencies. However, a CCD is the better choice for nonlinear scattering techniques as there is no need for time-consuming changing of the spectrometer to collect a full spectrum. Lastly the authors discuss the detection sensitivity of the SHS signal and outlooks for the topic as they stood then. They showed that due to the high-performance nature of their SHS system, such signals would be readily detectable from a single droplet suspended in the air under the correct conditions. It was also determined that by using a fs IR pulse with 2.0 μJ energy and a ps visible pulse at 10μJ and 50 kHz, VSFS could be measured with their current setup. With the experimental setup for SHS from aerosol surfaces now optimized, the next steps were to study the ways that atmospherically relevant conditions effected the droplet surface properties.

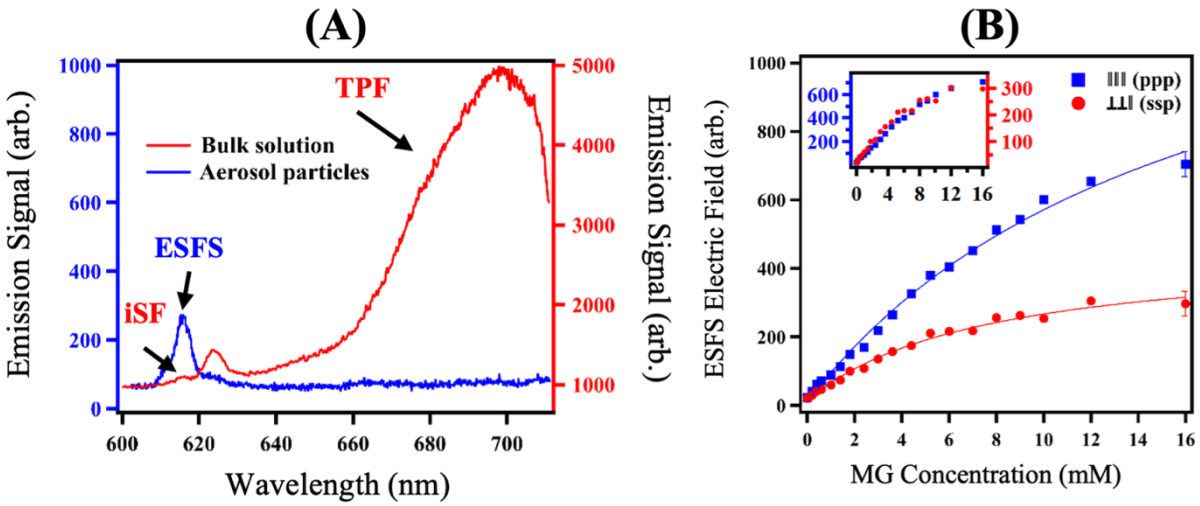

Figure 7. (A) Parametric emission spectra from aerosol droplet (blue) and bulk solution (red) samples containing Malachite Green in 1.0 M NaCl under excitation from 1030 nm SWIR pulses. (B) PPP (blue) and SSP (red) polarized ESFS electric fields versus concentration of MG in the bulk solution.
Adapted with permission from Ref. 85. Copyright 2020 American Chemical Society.

Since aerosol droplets exist in a variable environment and naturally contain different salt concentrations, it is important to understand the ways that these variables impact droplet surfaces. Efforts were conducted in 2019 to use SHS to understand the effects of surrounding relative humidity and salt concentration on organic species at droplet surfaces in air.[90] Using the previously optimized experimental setup, spectra were collected from nano-droplet and bulk samples of DiA4 in 1.0 M NaCl using the same stock solution. The spectrum from the droplet sample showed a strong peak at 2ω, coherent SHS, and a comparatively weak TPF peak near 620 nm. The bulk spectrum also shows two peaks: one at 2ω and the other 620 nm, with the former being from incoherent HRS and weaker than the latter from TPF. To investigate the effects of relative humidity on droplet surfaces, emission spectra were collected using droplets from the same solution surrounded by humidified N_2 either above (90%, blue trace) or below (40%, red trace) the deliquescence point of NaCl, as shown in Figure 6(A). Both spectra show sharp peaks at 2ω for SHS and broad signals at 620 nm for TPF. The spectrum collected at 90% RH gives the 2ω peak being much stronger than the TPF, while at 40% the proportions are reversed. Furthermore, the SHS peak at 40% is weaker than that at 90% and the TPF peak at 90% is less than that at 40%, confirming that surrounding humidity can dramatically affect both the surface and bulk of the particles. To assess the effects of salt concentration on the interfacial adsorption affinity of DiA4, SHS intensities were measured at 0.1, 0.5, and 1.0 M NaCl and increasing DiA4 concentrations. It is shown in Figure 6(B) that the isotherms are nearly collinear with increasing concentrations, suggesting that the interfacial adsorption constants are similar at different salt concentrations. As demonstrated previously with SHS from particles in dispersive media, the free energy of interfacial adsorption can be readily calculated from SHS isotherm data.[61] Rao et al used this Langmuir

adsorption model to show that the calculated adsorption coefficients for DiA4 at droplet surfaces increased with increasing RH. However, after calculating free energies of adsorption from these data, there was no significant effect in interfacial affinity for DiA4. The SHS experiments also offer valuable information in terms of the number of interfacial adsorption sites, which were shown to increase with relative humidity. The results from this work further demonstrated the utility of SHS from both spectroscopic and chemical viewpoints. However, SHS still cannot identify

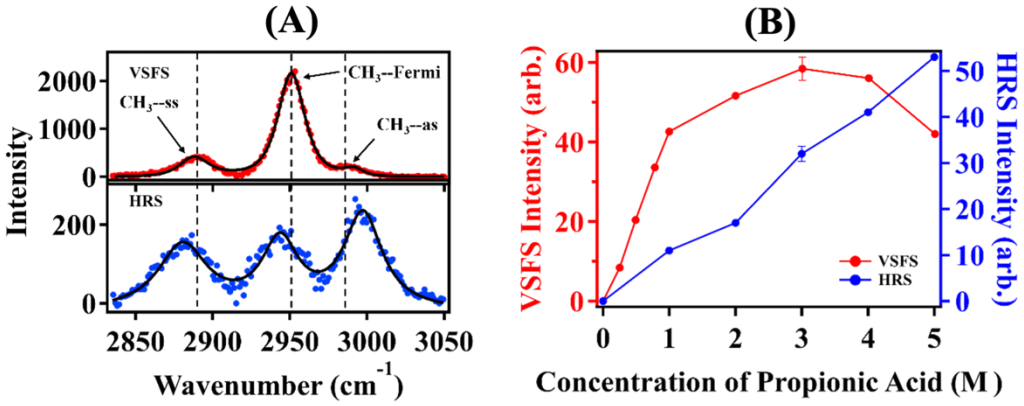

Figure 8. (A) VSFS (red, top) and hyper-Raman (blue, bottom) spectra from aerosol droplets from a stock solution of 4.0 M propionic acid in 0.5 M NaCl. (B) VSFS (red, left axis) and hyper-Raman (blue, right axis) intensities from the asymmetric methyl stretch at different concentrations of propionic acid.
Reprinted in part with permission from{Qian, Y., Brown, J.B., Huang-Fu, ZC., Zhang, T., Wang, H., Wang, SY., Dadap, J.I., Rao, Y. In situ analysis of the bulk and surface chemical compositions of organic aerosol particles. *Commun. Chem.* **2022**, 5, 58.}. Copyright {2022} The Author(s). This is an open access article distributed under the terms of the Creative Commons CC BY license, https://www.nature.com/articles/s42004-022-00674-8#citeas

interfacial species, describe molecular orientation at the surface, and is restricted in its applicable systems since resonance enhanced SHS depends on both incident frequency as well as molecular electronic properties.

The development of SHS from droplets in air should not be viewed as a necessary milestone to further the fields of nonlinear optics and surface chemistry, but a development of an analytical technique with its own merits and application potentials. For instance, SHS was shown early on to be capable of determining surface charge densities and surface electrostatic potentials. A variation of SHS, electric field-induced SHG has been shown to use the third-order susceptibility, $\chi^{(3)}$, to observe charges at interfaces.[55] This method may also be extended to droplets in air to study the charged nature of aerosol surfaces. SHS experiments conducted on droplets in the air have also demonstrated the most intense signal out of the three techniques discussed in this article. For this reason, SHS is the ideal method for studying dynamic electrical processes at droplet surfaces with fast time resolution. Additionally, the high-performance nature of the optimized SHS system for droplets in air has the potential to observe scattering signals from just one droplet suspended in air.[85]

Electronic sum-frequency scattering (ESFS) from droplet surfaces in air.

While second-harmonic spectroscopies have been employed extensively over the past few decades, a shortcoming of the technique is that it can only provide spectral information by tuning the laser wavelength point by point.[94] However, this problem was remedied nearly twenty years ago with the introduction of electronic sum-frequency generation (ESFG), when Yamaguchi and Tahara mixed white light continuum with their 800 nm pulse to produce broadband SF signals in the visible range, effectively extending the applicability of SHG to more chromophore systems.[95] This method has since been thoroughly developed and applied to extract electronic information from diverse systems. [96-99]

After the development of SHS from airborne droplets, the natural evolution to ESFS proceeded in order to extract more information about nanodroplet surfaces. ESFS from droplets surfaces was achieved by mixing a ps 1030 nm near-IR pulse with a tunable fs SWIR pulse from 1415 to 1670 nm.[85] When using droplets generated from a solution of 1.0 M NaCl with 200 μM malachite green (MG), Rao et al were able to observe the parametric emission spectrum of MG at $\omega_{ESFS} = \omega_{1030\ nm} + \omega_{SWIR}$ in the bulk phase and at the droplet surface as shown in Figure 7(A). Comparing the droplet surface and solution bulk emission spectra from 600 to 710 nm showed that the ESFS signal from the droplets was in fact the coherent signal from their surface, based off peak ratios of TPF and incoherent ESFS. One of the most useful properties of sum-frequency spectroscopy is the utilization of polarization combinations to uncover orientational information.[80] Comparing the *ppp* and *ssp* polarization combination ESFS spectra for MG at droplet surfaces showed that the *ppp* peak was over 3x stronger than the corresponding *ssp* peak. This difference in intensity and lack of peak position change suggest that the MG molecules exist at droplet surfaces in an ordered fashion: interfacial MG molecules at the droplet surface all have a qualitatively similar orientation relative to the surface normal. Furthermore, comparing the ESFS spectrum from the droplet sample with the UV-vis absorption spectrum from the bulk shows a 5 ± 1 nm shift in the peak location, which indicates that the solvation energy at the droplet surfaces is greater than in the bulk. This suggests that the droplet surfaces are less polar, i.e., more hydrophobic, than the bulk solution, which can influence chemical activity at these curved surfaces. Comparing the electric field intensities for ESFS spectra collected at *ppp* and *ssp* polarization combinations at increasing MG stock concentrations produced the two Langmuir-type adsorption isotherms shown in Figure 7(B). For all MG concentrations, the *ppp* was greater than the *ssp*, with the two being nearly collinear after normalization. This suggests that there was no considerable orientational change for MG at the droplet surfaces for concentrations less than 16 mM. Additionally, fitting of the isotherms to the Langmuir adsorption model allowed the calculation of the free energy of adsorption to the droplet surface, which is lower than that for the planar surface,[100] and was attributed to the highly curved droplet surface. While the development of ESFS was a significant step for nonlinear optical spectroscopy, it proved to be a time-consuming process, requiring tuning of the IR pulse to form a spectrum, and still not providing *in situ* chemical identification for droplets in air.

Electronic SFS has advantages over SHS in that it broadens the range of usable chromophores by introducing a tunable broadband short-wave IR beam. Furthermore, the addition of the third beam to the system allows the use of multiple polarization combinations to extract more information about the electronic properties of droplet surfaces. ESFS also has a more intense signal from droplet surfaces than its vibrational counterpart which improves experimental efficiency. As it was with other interfaces, ESFS may also be a candidate for the introduction of time resolution and spectral resolution which can provide ultrafast time resolution of interfacial processes as well

as direct observations of the complex nature of the SFG signal.[101, 102] Since ESFS is inherently sensitive to interfaces, an interesting application would be its use to observe charge transfer and relaxation processes at buried interfaces, such as that in semiconducting nanoparticles with core-shell construction; combined with trapping techniques to observe the system unencumbered by solvents or substrates.[96, 102]

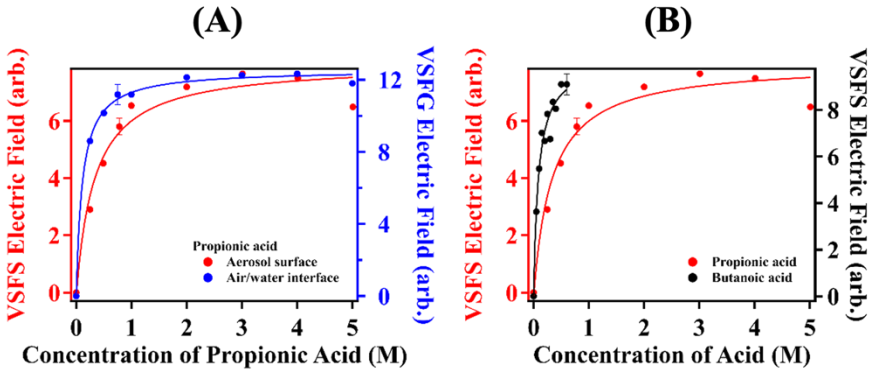

Figure 9. (A) VSFS (red, left) and VSFG (blue, right) electric fields versus concentration of propionic acid in 0.5 M NaCl. (B) VSFS electric field versus concentration of acid in 0.5 M NaCl stock solution for propionic acid (red, left) and butanoic acid (black, right).
Reprinted with permission from {Qian, Y., Brown, J.B., Huang-Fu, ZC., Zhang, T., Wang, H., Wang, SY., Dadap, J.I., Rao, Y. In situ analysis of the bulk and surface chemical compositions of organic aerosol particles. *Commun. Chem.* **2022**, 5, 58.}. Copyright {2022} The Author(s). This is an open access article distributed under the terms of the Creative Commons CC BY license, https://www.nature.com/articles/s42004-022-00674-8#citeas

Vibrational sum-frequency scattering (VSFS) from droplet surfaces in air.

The decades-long goal of vibrational sum-frequency scattering from droplets in air was achieved in 2022 by Rao et al.[77] Using a ps 1030 nm pulse and an OPA to generate a tunable fs IR pulse from 2500 to 4500 nm, the authors collected the interfacial vibrational spectrum of propionic acid molecules at the surface of droplets generated from a solution of 0.5 M NaCl and 4.0 M propionic acid. By collecting the generated signals in both forward and perpendicular propagating directions, the VSFS from the droplet surface at 90° and hyper-Raman from the droplet bulk at 0° were observed. These interfacial and bulk spectra are shown in the top and bottom panels of Figure 8(A), respectively. The VSFS spectrum showed three distinct vibrational modes which aligned with the selection rules from planar VSFG experiments.[103] The hyper-Raman spectrum from the same sample also showed three distinct modes with the same vibrational assignments. To confirm that the VSFS signal was from the droplet surface and the hyper-Raman signal was from the droplet bulk, spectra were collected at increasing propionic acid concentrations. Their intensities at increasing propionic acid concentrations are shown in Figure 8(B). The hyper-Raman intensity (blue, right axis) increases linearly with propionic acid concentration while the VSFS (red, left axis) follows a Langmuir-type trend, supporting their respective bulk and surface labels. Polarization-resolved VSFS spectra were also collected for these propionic acid containing

droplets to investigate interfacial orientation. Comparing the HHH, HVV, VHV, and VVH polarization combinations (H: horizontal, V: vertical, in increasing wavelength order), revealed a qualitative agreement with previous VSFS theories—only HHH and VVH produced a signal, HVV and VHV produced no spectra—however, after relating the experimental and theoretical hyperpolarizabilities, there was a fundamental disagreement. Nevertheless, the apparent spectra from HHH and VVH polarizations and the lack thereof for other combinations suggests that the acid molecules exist at the droplet surfaces in an ordered manner. As it has been done previously for SHS and ESFS, and since it can provide valuable information from experiments of scattering in dispersive media, adsorption isotherms were conducted for propionic acid at droplet surfaces using VSFS and at the bulk solution surface using VSFG. The comparison of VSFS and VSFG isotherms of propionic acid are shown in Figure 9(A). By fittings to the Langmuir adsorption model, adsorption free energies were calculated, with the ΔG being lower at droplet surfaces versus the planar analog, echoing the ESFS results. Further confirmation that the adsorption of organics to the curved droplet surfaces is restricted relative to the bulk planar surfaces suggests that the two systems should not be used interchangeably. Using VSFS, an isotherm was also conducted for butanoic acid under the same experimental conditions, as shown in Figure 9(B). The butanoic acid VSFS isotherm produced a ΔG value higher than that for propionic acid, enforcing that larger, more hydrophobic molecules have an increased surface affinity for both droplets and bulk systems. The development of VSFS from droplet surfaces in the air with simultaneous detection of hyper-Raman spectra from the underlying bulk marked a very significant milestone in both nonlinear optics and surface chemistry.

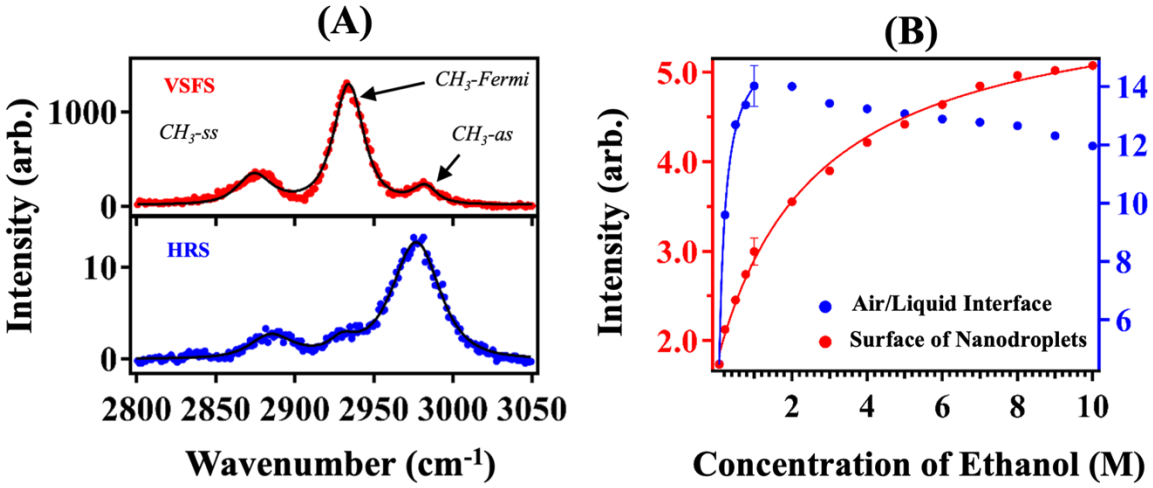

Figure 10. (A) VSFS (red, top) and hyper-Raman (blue, bottom) spectra from aerosol droplets generated from 10 M ethanol in 0.5 M NaCl stock solution. (B) VSFS (red, left) and VSFG (blue, right) electric field versus concentration of ethanol in 0.5 M NaCl stock solution.
Adapted with permission from Ref. 78. Copyright 2022 American Chemical Society.

As an essential trait of the technique, the ability of VSFS to identify molecular species at droplet surfaces in air must be explored. Shortly after its development, VSFS was used to investigate the behaviors of n-alcohols (C = 1 to 4) at droplet surfaces.[78] To begin, the dual utility of the method was demonstrated using droplets generated from a stock solution of 10 M ethanol in 0.5 M NaCl, showing VSFS and hyper-Raman spectra from the droplet surface and underlying

bulk, respectively, as shown in Figure 10(A). Using a stock solution of 0.5 M NaCl for VSFS instead of 1.0 M NaCl as previously used produced droplets with a diameter centered around 40 nm, a lognormal distribution from 10 to 300 nm, and a density of 3.8×10^6 cm^{-3}. This HHH polarized VSFS spectrum exhibited three peaks at 2879.7, 2932.8, and 2981.3 cm^{-1}, labeled according to VSFG selection rules as the methyl and ethyl symmetric stretching combination, the methyl Fermi resonance, and the methyl asymmetric/ethyl Fermi resonance combination, with the Fermi peak being the most intense. The hyper-Raman spectrum obtained from the same sample contained peaks for the symmetric methyl stretch, methyl Fermi resonance, and asymmetric methyl stretching modes at 2887.9, 2930.1, 2977.7, respectively, with the asymmetric peak being more intense than the other two. The relative differences in peak intensities between the VSFS and hyper-Raman spectra may be a result of molecular ordering differences: random within the droplet and more ordered at its surface. Considering the other three polarizations of VSFS spectra, the HVV spectrum contains a very weak asymmetric methyl stretching peak, the VHV spectrum contains no discernable features, and the VVH spectrum shows the symmetric methyl stretching mode and a stronger methyl Fermi resonance peak. Since the theory for molecular orientation at the tightly curved submicron droplet surface is not yet complete, only a qualitative conclusion may be drawn from these results: the ethanol molecules exist at the droplet surfaces in an ordered state. Using the VVH polarization combination, it was shown that VSFS spectra can clearly discern between methanol, ethanol, 1-propanol, and 1-butanol at droplet surfaces, and that the spectral selection rules developed for the planar surface can be extended to droplets in the air. Lastly, concentration isotherms were conducted for samples of ethanol in 0.5 M NaCl at droplet and planar solution surfaces, using VSFS and VSFG, respectively. While both followed a Langmuir-type trend the VSFS isotherm increased gradually while it reached a maximum early on for VSFG. Fittings of these curves to the Langmuir adsorption model gave adsorption constant values from which ΔG of adsorption values were calculated. The value for the planar surface was twice that of the droplet surface. The results in this report solidified VSFS as an analytical technique for studying chemistry at droplet surfaces in the air, from the identification of organics to their interfacial affinity. However, essential physical understandings of the technique are still missing such as detection limit, conversion efficiency, scattering patterns, and quantification of molecular orientation. Current efforts are underway by our group to fill the gaps by understanding nonlinear optical scattering from droplets from the ground up, as well as to assess the experimental efficacy of our VSFS system to improve it and guide others in the field.

The hallmark advantage of VSFS over SHS and ESFS is its ability to observe vibrational modes of molecules at droplet surfaces, thereby offering species identification and/or characterization. With this ability, VSFS is well suited for the observation of chemical reactions and dynamic processes at droplet surfaces, like it has done at the planar surface repetitiously.[55, 56, 65] For this reason, there are numerous pathways for potential uses of VSFS to investigate chemical reactions at droplet and particle surfaces *in situ*. For example, organic peroxides, common atmospheric reaction products which store and transport reactive radical species with active particle partitioning, may be fit to be studied by VSFS.[104] Due to their affinity for particle partitioning, VSFS may provide valuable insights into interfacial processes of organic peroxides which govern their environmental impacts. Gas uptake processes are essential to atmospheric chemistry. This processes which necessarily involves the gas/aerosol particle interface, leads to interfacial and bulk chemical processes with environmental impacts. The combination of VSFS for the droplet surface and hyper-Raman scattering for the particle bulk may be useful in

complimenting other observations of reactive uptake, such as that of ozone for reactions with small multifunctional acids and long-chained fatty acids, which have not been observed *in situ* from both bulk and interfacial perspectives. Current efforts are underway to use VSFS to observe gas-phase uptake to droplet surfaces with goals of introducing reaction processes, humidity, salt concentration, and particle size variables to form a more robust understanding of these relevant atmospheric and environmental processes.

Outlook

The demonstrations in this feature article of nonlinear optical scattering from droplets through SHS, ESFS, and VSFS have marked significant milestones in both nonlinear optics and surface chemistry. However, there is still room for improvement to the techniques. Due to weak signals from low density aerosol particles, new strategies are required to improve detection sensitivity.

Further improvements for Second-Order Scattering.

Improvements to SHS. SHS from aerosols has two main advantages over SFS that will lend to using SHS to develop a more fundamental understanding of second-order scattering: 1) experimental simplicity with only one incident beam; 2) the most intense scattered signal from aerosol surfaces. It should however be noted that there is still room for improvement in the detection efficiency of the SHS experiments. Such improvements could come from modernizing the detection system and optimizing the collection optics. The advantages of the SHS method make it the perfect technique for performing surface-specific, size-resolved, scattering angle experiments. Such experiments would lay the groundwork for developing a general theoretical model for second-order scattering from droplets in air. The high signal intensity and relative ease of experiments would allow for the use of lower concentration monodisperse aerosols in the scattering experiments for mapping scattering patters with high angular resolution. Such experiments would also allow the determination of an expression for the expected SH signal from different aerosol systems, as was done with planar SHG,[65] to guide others to employ the method in new and innovative ways.

Improvements to ESFS. ESFS holds an advantage over SHS in that the SWIR pulse allows for more diverse applications with resonance enhancement. The largest current hurdle with ESFS is that when using a narrowband SWIR pulse, the OPA must be tuned point-by-point to collect an entire spectrum which significantly impacts experimental efficiency.[85] As a remedy, a broadband-OPA might be used as has been in previous ESFG experiments from planar interfaces.[97-99, 102] With such an improvement, ESFS could likely be used for size-dependent angle-resolved scattering experiments like SHS but with the added variable of polarization. Such angle-resolved experiments may bridge the gap between SHS and VSFS theory and guide the community to a more robust understanding of these processes.

Improvements to VSFS. Having the weakest collected signal intensity from aerosol surfaces out of the three techniques, there is plenty of room for improvement to VSFS. The simplest improvement to the VSFS experiments would be to increase the incident pulse power and thereby increase the signal intensity with a higher-powered laser. Improvements can also be made to the detection system of our current VSFS setup. A state-of-the-art CCD detector and spectrometer would likely

improve experimental efficiency. Even with these improvements, size-dependent angle-resolved VSFS experiments would still be difficult. In addition, often-used heterodyne detection in planar surfaces could be adopted to speed up VSFS detection.[105-110] It is our hope that these efforts would allow the technique to observe interfacial reactions in the near future.

Angle-dependent Second-Order Scattering Experiments.

Aside from quantifying orientation across all particle and droplet surfaces, other fundamental considerations must be addressed to advance the second-order scattering field into maturity. For instance, light scattering profiles have not been mapped for scattered light form droplets or particles in the air. So called "angle-dependent" scattering measurements allow cross-referencing of experimental findings and theoretical models. Just as considering refractive index miss-matching affected the scattering pattern for experiments in dispersive media previously,[75] it would be naïve to assume that a difference in refractive indices between dispersive media and air would not also affect scattering patterns. Additionally, the fundamental differences in scattering process due to particle size, *i.e*., Mie scattering vs. Rayleigh scattering, must needs be considered through size-dependent mapping of scattering patters. To complete this task, and to develop a robust understanding of the second-order nonlinear scattering process, our group is devoting efforts to conducting angle-dependent SHS and SFS experiments. Since SHS is the simplest of the three techniques in execution and theory, we feel that this is the optimal starting ground. Such efforts will be extended step-by-step to the more complex systems of ESFS and VSFS as our understanding and experimental technologies continue to advance.

Size-Dependent Second-Order Scattering Studies.

Size-dependent surface-specific studies of droplets are essential in understanding the effects of droplet size on chemical processes and physical properties therein. An extreme experimental difficulty arises for size dependent nonlinear scattering: to obtain nearly monodisperse droplets for analysis, one must use a classifier-type filter which can have output efficiencies as low as 1%. Using SHS as a starting ground because of its high signal intensity, we plan to use narrow size distributions of aqueous droplets to study both the SHS scattering pattern as well as the effects of droplet size on molecular adsorption processes at droplet surfaces. By using several narrow size distributions, we will be able to understand the effects of droplet size on its surface properties in a robust and complete manner. This would, however, only provide information about surface adsorption from the particle bulk to its surface. By using the high performance VSFS and simultaneous hyper-Raman combination, we would be able to develop a size-dependent understanding of droplet chemical processes, both at the surface and within the droplet. Additionally, our preliminary results show promise in observations of gas phase adsorption of organics to unoccupied particle surfaces using VSFS. An interesting prospect for these experiments would be to investigate the dependence of organic uptake on relative humidity and salt concentrations, as both can affect droplet size and surface tension. The combination of narrow size distribution with VSFS would provide robust analyses of surface adsorption, from within or without, including adsorption/desorption isotherms, reaction kinetics and dynamics analyses, molecular orientation, size dependence, and even competitive adsorption in mixed systems.

Chemical Reactions at Droplet surfaces.

As an interface-specific vibrational spectroscopy, VSFS could be used to monitor chemical reactions at droplet surfaces. In a simple reaction, VSFS could be used to study acid/base chemistry

at droplet surfaces by observing deprotonation of gas phase acids at the surface of droplets whose bulk pH is controlled. in another example, using an oleate salt in the aerosols which would migrate to the droplet surface and a separate flow containing ozone, VSFS could possibly be used to observe the oxidation of the long carbon chain at the droplet surface. Similar to ozonolysis studies, VSFS could also be used to observe heterogeneous hydroxyl radical reactions at aerosol surfaces.[18] To observe such heterogenous reactions at droplet surfaces, VSFS must first be extended beyond observing the methyl stretching mode as it has currently been reported.[77, 78] This can increase experimental difficulty as increasing the output wavelength from an OPA also results in lower pulse energy. Additionally, a modified flow system would need to be implemented to introduce the gas phase and aerosol species to each other in a controlled manner. If constructed with plans in mind for studying reaction kinetics and dynamics, this flow system should be able to control the interaction time between the two phases. Additionally, all of these potential experiments would be prime for investigating the effects of relative humidity and salt concentration, as it was demonstrated with SHS.[90]

Summary

In this feature article, we focused on second-order nonlinear optical techniques recently extended to study the unique surface properties of small droplets in the air. We first discussed the basic process of surface adsorption to droplet surfaces and described the development of nonlinear scattering from droplets in solution. The development of SHS from aerosol droplets was then discussed and important observations were made about the impact of ambient humidity on interfacial solute adsorption for droplets in air. ESFS from droplets in air was shown to uncover solvation information at droplet surfaces and extend the applicability of SHS. Next, the development of VSFS for chemical identification was described and it was shown that the technique uncovered restricted solute adsorption to the droplet surface relative to the bulk surface. The advantages and pitfalls of the SHS, ESFS, and VSFS techniques were discussed as well as potential improvements. Lastly, our visions for the future directions of nonlinear scattering from droplets in the air were discussed, including single particle, size-resolved, and angle-resolved measurements, as well as *in-situ* monitoring of reactions and how they may be achieved. These state-of-the-art surface-specific techniques have many applications in studying small droplet systems and could be an indispensable tool for researchers from biology to catalysis and synthesis to atmospheric chemistry. We hope that this entry has educated a broad audience on the importance and ubiquity of nano-droplet and micro-droplet surfaces as well as the current standing of second-order nonlinear scattering techniques.

Notes

The authors declare no competing financial interests.

Authors Contributions

*Corresponding author: yi.rao@usu.edu
#J.B.B. and Y.Q.Q. contributed equally to this work.

Acknowledgements

This material is based upon work supported by the National Science Foundation under Grant No. [2203983].

References

(1) Shimizu, J.; Endoh, R.; Fukuda, T.; Inagaki, T.; Hano, H.; Asami, R.; Kawabata, K.-i.; Yokoyama, M.; Furuhata, H. Safety evaluation of superheated perfluorocarbon nanodroplets for novel phase change type neurological therapeutic agents. *Perspectives in Medicine* **2012**, *1* (1), 25-29. DOI: https://doi.org/10.1016/j.permed.2012.02.058.

(2) Kee, A. L. Y.; Teo, B. M. Biomedical applications of acoustically responsive phase shift nanodroplets: Current status and future directions. *Ultrasonics Sonochemistry* **2019**, *56*, 37-45. DOI: https://doi.org/10.1016/j.ultsonch.2019.03.024.

(3) Kandadai, M. A.; Mohan, P.; Lin, G.; Butterfield, A.; Skliar, M.; Magda, J. J. Comparison of Surfactants Used to Prepare Aqueous Perfluoropentane Emulsions for Pharmaceutical Applications. *Langmuir* **2010**, *26* (7), 4655-4660. DOI: 10.1021/la100307r.

(4) Chang, N.; Lu, S.; Qin, D.; Xu, T.; Han, M.; Wang, S.; Wan, M. Efficient and controllable thermal ablation induced by short-pulsed HIFU sequence assisted with perfluorohexane nanodroplets. *Ultrasonics Sonochemistry* **2018**, *45*, 57-64. DOI: https://doi.org/10.1016/j.ultsonch.2018.02.033.

(5) Liu, T.; Abbatt, J. P. Oxidation of sulfur dioxide by nitrogen dioxide accelerated at the interface of deliquesced aerosol particles. *Nature Chemistry* **2021**, *13* (12), 1173-1177.

(6) Dyett, B. P.; Zhang, X. Accelerated Formation of H2 Nanobubbles from a Surface Nanodroplet Reaction. *ACS Nano* **2020**, *14* (9), 10944-10953. DOI: 10.1021/acsnano.0c03059.

(7) Wei, Z.; Li, Y.; Cooks, R. G.; Yan, X. Accelerated Reaction Kinetics in Microdroplets: Overview and Recent Developments. *Annual Review of Physical Chemistry* **2020**, *71* (1), 31-51. DOI: 10.1146/annurev-physchem-121319-110654 (acccessed 2023/03/21).

(8) Reid, J. P.; Sayer, R. M. Heterogeneous atmospheric aerosol chemistry: laboratory studies of chemistry on water droplets. *Chemical Society Reviews* **2003**, *32* (2), 70-79, 10.1039/B204463N. DOI: 10.1039/B204463N.

(9) Nam, I.; Nam, H. G.; Zare, R. N. Abiotic synthesis of purine and pyrimidine ribonucleosides in aqueous microdroplets. *Proceedings of the National Academy of Sciences* **2018**, *115* (1), 36-40. DOI: 10.1073/pnas.1718559115 (acccessed 2023/03/21).

(10) Zhou, Z.; Yan, X.; Lai, Y.-H.; Zare, R. N. Fluorescence Polarization Anisotropy in Microdroplets. *The Journal of Physical Chemistry Letters* **2018**, *9* (11), 2928-2932. DOI: 10.1021/acs.jpclett.8b01129.

(11) Geiger, F. M.; McNeill, V. F.; Orr-Ewing, A. J. Virtual Issue on Atmospheric Aerosol Research. *The Journal of Physical Chemistry A* **2022**, *126* (32), 5233-5235. DOI: 10.1021/acs.jpca.2c04827.

(12) Morris, H. S.; Grassian, V. H.; Tivanski, A. V. Humidity-dependent surface tension measurements of individual inorganic and organic submicrometre liquid particles. *Chemical science* **2015**, *6* (5), 3242-3247. DOI: https://doi.org/10.1039/C4SC03716B.

(13) Ruehl, C. R.; Wilson, K. R. Surface Organic Monolayers Control the Hygroscopic Growth of Submicrometer Particles at High Relative Humidity. *The Journal of Physical Chemistry A* **2014**, *118* (22), 3952-3966. DOI: 10.1021/jp502844g.
(14) Corral Arroyo, P.; David, G.; Alpert, P. A.; Parmentier, E. A.; Ammann, M.; Signorell, R. Amplification of light within aerosol particles accelerates in-particle photochemistry. *Science* **2022**, *376* (6590), 293-296. DOI: doi:10.1126/science.abm7915.
(15) Marcolli, C.; Krieger, U. K. Relevance of Particle Morphology for Atmospheric Aerosol Processing. *Trends in Chemistry* **2020**, *2* (1), 1-3. DOI: https://doi.org/10.1016/j.trechm.2019.11.008.
(16) Shrivastava, M.; Cappa, C. D.; Fan, J.; Goldstein, A. H.; Guenther, A. B.; Jimenez, J. L.; Kuang, C.; Laskin, A.; Martin, S. T.; Ng, N. L.; et al. Recent advances in understanding secondary organic aerosol: Implications for global climate forcing. *Reviews of Geophysics* **2017**, *55* (2), 509-559. DOI: https://doi.org/10.1002/2016RG000540.
(17) Mishra, H.; Enami, S.; Nielsen, R. J.; Hoffmann, M. R.; Goddard, W. A.; Colussi, A. J. Anions dramatically enhance proton transfer through aqueous interfaces. *Proceedings of the National Academy of Sciences* **2012**, *109* (26), 10228-10232. DOI: doi:10.1073/pnas.1200949109.
(18) McNeill, V. F. Aqueous Organic Chemistry in the Atmosphere: Sources and Chemical Processing of Organic Aerosols. *Environmental Science & Technology* **2015**, *49* (3), 1237-1244. DOI: 10.1021/es5043707.
(19) Nozière, B.; Baduel, C.; Jaffrezo, J.-L. The dynamic surface tension of atmospheric aerosol surfactants reveals new aspects of cloud activation. *Nature Communications* **2014**, *5* (1), 3335. DOI: 10.1038/ncomms4335.
(20) Casillas-Ituarte, N. N.; Callahan, K. M.; Tang, C. Y.; Chen, X.; Roeselová, M.; Tobias, D. J.; Allen, H. C. Surface organization of aqueous MgCl₂ and application to atmospheric marine aerosol chemistry. *Proceedings of the National Academy of Sciences* **2010**, *107* (15), 6616-6621. DOI: doi:10.1073/pnas.0912322107.
(21) McNeill, V. F.; Sareen, N.; Schwier, A. N. Surface-active organics in atmospheric aerosols. *Atmospheric and aerosol chemistry* **2014**, 201-259. DOI: https://doi.org/10.1007/128_2012_404.
(22) Tolman, R. C. The Effect of Droplet Size on Surface Tension. *The Journal of Chemical Physics* **1949**, *17* (3), 333-337. DOI: 10.1063/1.1747247.
(23) Xue, Y.-Q.; Yang, X.-C.; Cui, Z.-X.; Lai, W.-P. The Effect of Microdroplet Size on the Surface Tension and Tolman Length. *The Journal of Physical Chemistry B* **2011**, *115* (1), 109-112. DOI: 10.1021/jp1084313.
(24) Morris, H. S.; Grassian, V. H.; Tivanski, A. V. Correction: Humidity-dependent surface tension measurements of individual inorganic and organic submicrometre liquid particles. *Chemical science* **2015**, *6* (10), 6021-6021. DOI: 10.1039/C5SC90044A.
(25) McMurry, P. H. A review of atmospheric aerosol measurements. *Atmospheric Environment* **2000**, *34* (12), 1959-1999. DOI: https://doi.org/10.1016/S1352-2310(99)00455-0.
(26) Shen, Y. R. *Fundamentals of Sum-Frequency Spectroscopy*; Cambridge University Press, 2016.
(27) Lee, H. D.; Tivanski, A. V. Atomic Force Microscopy: An Emerging Tool in Measuring the Phase State and Surface Tension of Individual Aerosol Particles. *Annual Review of Physical Chemistry* **2021**, *72* (1), 235-252. DOI: 10.1146/annurev-physchem-090419-110133 (acccessed 2023/05/04).

(28) Ko, H.; Singamaneni, S.; Tsukruk, V. V. Nanostructured Surfaces and Assemblies as SERS Media. *Small* **2008**, *4* (10), 1576-1599. DOI: https://doi.org/10.1002/smll.200800337.
(29) Konovalov, O. V.; Belova, V.; La Porta, F.; Saedi, M.; Groot, I. M.; Renaud, G.; Snigireva, I.; Snigirev, A.; Voevodina, M.; Shen, C. X-ray reflectivity from curved surfaces as illustrated by a graphene layer on molten copper. *Journal of Synchrotron Radiation* **2022**, *29* (3). DOI: https://doi.org/10.1107/S1600577522002053.
(30) Festersen, S.; Hrkac, S. B.; Koops, C. T.; Runge, B.; Dane, T.; Murphy, B. M.; Magnussen, O. M. X-ray reflectivity from curved liquid interfaces. *Journal of Synchrotron Radiation* **2018**, *25* (2), 432-438. DOI: https://doi.org/10.1107/S1600577517018057.
(31) Powell, C. J.; Jablonski, A. Surface sensitivity of X-ray photoelectron spectroscopy. *Nuclear Instruments and Methods in Physics Research Section A: Accelerators, Spectrometers, Detectors and Associated Equipment* **2009**, *601* (1), 54-65. DOI: https://doi.org/10.1016/j.nima.2008.12.103.
(32) Odom, R. W.; Schueler, B. *Laser microprobe mass spectrometry: Ion and neutral analysis*; Oxford University Press, 1990.
(33) Wouters, L.; Van Grieken, R.; Linton, R.; Bauer, C. Discrimination between coprecipitated and adsorbed lead on individual calcite particles using laser microprobe mass analysis. *Analytical Chemistry* **1988**, *60* (20), 2218-2220. DOI: https://doi.org/10.1021/ac00171a011.
(34) Fu, Y.; Kuppe, C.; Valev, V. K.; Fu, H.; Zhang, L.; Chen, J. Surface-Enhanced Raman Spectroscopy: A Facile and Rapid Method for the Chemical Component Study of Individual Atmospheric Aerosol. *Environmental Science & Technology* **2017**, *51* (11), 6260-6267. DOI: 10.1021/acs.est.6b05910.
(35) Olson, N. E.; Xiao, Y.; Lei, Z.; Ault, A. P. Simultaneous Optical Photothermal Infrared (O-PTIR) and Raman Spectroscopy of Submicrometer Atmospheric Particles. *Analytical Chemistry* **2020**, *92* (14), 9932-9939. DOI: 10.1021/acs.analchem.0c01495.
(36) Finlayson-Pitts, B. J. Reactions at surfaces in the atmosphere: integration of experiments and theory as necessary (but not necessarily sufficient) for predicting the physical chemistry of aerosols. *Physical Chemistry Chemical Physics* **2009**, *11* (36), 7760-7779. DOI: https://doi.org/10.1039/B906540G.
(37) Jacobs, M. I.; Xu, B.; Kostko, O.; Wiegel, A. A.; Houle, F. A.; Ahmed, M.; Wilson, K. R. Using Nanoparticle X-ray Spectroscopy to Probe the Formation of Reactive Chemical Gradients in Diffusion-Limited Aerosols. *The Journal of Physical Chemistry A* **2019**, *123* (28), 6034-6044. DOI: 10.1021/acs.jpca.9b04507.
(38) Martinez, I. S.; Peterson, M. D.; Ebben, C. J.; Hayes, P. L.; Artaxo, P.; Martin, S. T.; Geiger, F. M. On molecular chirality within naturally occurring secondary organic aerosol particles from the central Amazon Basin. *Physical Chemistry Chemical Physics* **2011**, *13* (26), 12114-12122. DOI: https://doi.org/10.1039/C1CP20428A.
(39) Ebben, C. J.; Shrestha, M.; Martinez, I. S.; Corrigan, A. L.; Frossard, A. A.; Song, W. W.; Worton, D. R.; Petäjä, T.; Williams, J.; Russell, L. M.; et al. Organic Constituents on the Surfaces of Aerosol Particles from Southern Finland, Amazonia, and California Studied by Vibrational Sum Frequency Generation. *The Journal of Physical Chemistry A* **2012**, *116* (32), 8271-8290. DOI: 10.1021/jp302631z.
(40) Ebben, C. J.; Ault, A. P.; Ruppel, M. J.; Ryder, O. S.; Bertram, T. H.; Grassian, V. H.; Prather, K. A.; Geiger, F. M. Size-Resolved Sea Spray Aerosol Particles Studied by Vibrational Sum Frequency

Generation. *The Journal of Physical Chemistry A* **2013**, *117* (30), 6589-6601. DOI: 10.1021/jp401957k.
(41) Allen, H. C.; Gragson, D. E.; Richmond, G. L. Molecular Structure and Adsorption of Dimethyl Sulfoxide at the Surface of Aqueous Solutions. *The Journal of Physical Chemistry B* **1999**, *103* (4), 660-666. DOI: 10.1021/jp9820323.
(42) Rudd, B. A. W.; Vidalis, A. S.; Allen, H. C. Thermodynamic versus non-equilibrium stability of palmitic acid monolayers in calcium-enriched sea spray aerosol proxy systems. *Physical Chemistry Chemical Physics* **2018**, *20* (24), 16320-16332. DOI: https://doi.org/10.1039/C8CP01188E.
(43) Gordon, B. P.; Lindquist, G. A.; Crawford, M. L.; Wren, S. N.; Moore, F. G.; Scatena, L. F.; Richmond, G. L. Diol it up: The influence of NaCl on methylglyoxal surface adsorption and hydration state at the air–water interface. *The Journal of Chemical Physics* **2020**, *153* (16), 164705. DOI: https://doi.org/10.1063/5.0017803.
(44) Ault, A. P.; Zhao, D.; Ebben, C. J.; Tauber, M. J.; Geiger, F. M.; Prather, K. A.; Grassian, V. H. Raman microspectroscopy and vibrational sum frequency generation spectroscopy as probes of the bulk and surface compositions of size-resolved sea spray aerosol particles. *Physical Chemistry Chemical Physics* **2013**, *15* (17), 6206-6214. DOI: https://doi.org/10.1039/C3CP43899F.
(45) Rafferty, A.; Vennes, B.; Bain, A.; Preston, T. C. Optical trapping and light scattering in atmospheric aerosol science. *Physical Chemistry Chemical Physics* **2023**, *25* (10), 7066-7089. DOI: https://doi.org/10.1039/D2CP05301B.
(46) Carson, P. G.; Johnston, M. V.; Wexler, A. S. Real-time monitoring of the surface and total composition of aerosol particles. *Aerosol science and technology* **1997**, *26* (4), 291-300. DOI: https://doi.org/10.1080/02786829708965431.
(47) Rovelli, G.; Jacobs, M. I.; Willis, M. D.; Rapf, R. J.; Prophet, A. M.; Wilson, K. R. A critical analysis of electrospray techniques for the determination of accelerated rates and mechanisms of chemical reactions in droplets. *Chemical science* **2020**, *11* (48), 13026-13043. DOI: 10.1039/D0SC04611F.
(48) Shen, Y.-R. *The Principles of Nonlinear Optics*; John Wiley & Sons, 1984.
(49) Bloembergen, N.; Chang, R. K.; Lee, C. H. Second-Harmonic Generation of Light in Reflection from Media with Inversion Symmetry. *Physical Review Letters* **1966**, *16* (22), 986-989. DOI: 10.1103/PhysRevLett.16.986.
(50) Shen, Y. Optical second harmonic generation at interfaces. *Annual Review of Physical Chemistry* **1989**, *40* (1), 327-350. DOI: https://doi.org/10.1146/annurev.pc.40.100189.001551.
(51) Zhu, X. D.; Suhr, H.; Shen, Y. R. Surface vibrational spectroscopy by infrared-visible sum frequency generation. *Physical Review B* **1987**, *35* (6), 3047-3050. DOI: 10.1103/PhysRevB.35.3047.
(52) Eisenthal, K. B. Second Harmonic Spectroscopy of Aqueous Nano- and Microparticle Interfaces. *Chemical Reviews* **2006**, *106* (4), 1462-1477. DOI: 10.1021/cr0403685.
(53) Shen, Y. R. Phase-Sensitive Sum-Frequency Spectroscopy. *Annual Review of Physical Chemistry* **2013**, *64* (1), 129-150. DOI: 10.1146/annurev-physchem-040412-110110.
(54) Wang, H.-F.; Velarde, L.; Gan, W.; Fu, L. Quantitative Sum-Frequency Generation Vibrational Spectroscopy of Molecular Surfaces and Interfaces: Lineshape, Polarization, and Orientation. *Annual Review of Physical Chemistry* **2015**, *66* (1), 189-216. DOI: 10.1146/annurev-physchem-040214-121322.

(55) Geiger, F. M. Second Harmonic Generation, Sum Frequency Generation, and χ(3): Dissecting Environmental Interfaces with a Nonlinear Optical Swiss Army Knife. *Annual Review of Physical Chemistry* **2009**, *60* (1), 61-83. DOI: 10.1146/annurev.physchem.59.032607.093651.
(56) Jubb, A. M.; Hua, W.; Allen, H. C. Environmental Chemistry at Vapor/Water Interfaces: Insights from Vibrational Sum Frequency Generation Spectroscopy. *Annual Review of Physical Chemistry* **2012**, *63* (1), 107-130. DOI: 10.1146/annurev-physchem-032511-143811.
(57) Wang, H.; Yan, E. C. Y.; Borguet, E.; Eisenthal, K. B. Second harmonic generation from the surface of centrosymmetric particles in bulk solution. *Chemical Physics Letters* **1996**, *259* (1), 15-20. DOI: https://doi.org/10.1016/0009-2614(96)00707-5.
(58) Wang, H.; Yan, E. C. Y.; Liu, Y.; Eisenthal, K. B. Energetics and Population of Molecules at Microscopic Liquid and Solid Surfaces. *The Journal of Physical Chemistry B* **1998**, *102* (23), 4446-4450. DOI: 10.1021/jp980491y.
(59) Eckenrode, H. M.; Dai, H.-L. Nonlinear Optical Probe of Biopolymer Adsorption on Colloidal Particle Surface: Poly-l-lysine on Polystyrene Sulfate Microspheres. *Langmuir* **2004**, *20* (21), 9202-9209. DOI: 10.1021/la048863j.
(60) Tocci, G.; Liang, C.; Wilkins, D. M.; Roke, S.; Ceriotti, M. Second-Harmonic Scattering as a Probe of Structural Correlations in Liquids. *The Journal of Physical Chemistry Letters* **2016**, *7* (21), 4311-4316. DOI: 10.1021/acs.jpclett.6b01851.
(61) Wang, H.; Troxler, T.; Yeh, A.-G.; Dai, H.-L. In Situ, Nonlinear Optical Probe of Surfactant Adsorption on the Surface of Microparticles in Colloids. *Langmuir* **2000**, *16* (6), 2475-2481. DOI: 10.1021/la9909087.
(62) Srivastava, A.; Eisenthal, K. B. Kinetics of molecular transport across a liposome bilayer. *Chemical Physics Letters* **1998**, *292* (3), 345-351. DOI: https://doi.org/10.1016/S0009-2614(98)00662-9.
(63) Zeng, J.; Eckenrode, Heather M.; Dounce, Susan M.; Dai, H.-L. Time-Resolved Molecular Transport across Living Cell Membranes. *Biophysical Journal* **2013**, *104* (1), 139-145. DOI: https://doi.org/10.1016/j.bpj.2012.11.3814.
(64) Smolentsev, N.; Roke, S. Self-Assembly at Water Nanodroplet Interfaces Quantified with Nonlinear Light Scattering. *Langmuir* **2020**, *36* (31), 9317-9322. DOI: 10.1021/acs.langmuir.0c01887.
(65) Shen, Y. Surface properties probed by second-harmonic and sum-frequency generation. *Nature* **1989**, *337* (6207), 519-525. DOI: https://doi.org/10.1038/337519a0.
(66) Roke, S.; Roeterdink, W. G.; Wijnhoven, J. E. G. J.; Petukhov, A. V.; Kleyn, A. W.; Bonn, M. Vibrational Sum Frequency Scattering from a Submicron Suspension. *Physical Review Letters* **2003**, *91* (25), 258302. DOI: 10.1103/PhysRevLett.91.258302.
(67) de Aguiar, H. B.; de Beer, A. G. F.; Strader, M. L.; Roke, S. The Interfacial Tension of Nanoscopic Oil Droplets in Water Is Hardly Affected by SDS Surfactant. *Journal of the American Chemical Society* **2010**, *132* (7), 2122-2123. DOI: 10.1021/ja9095158.
(68) Smit, W. J.; Smolentsev, N.; Versluis, J.; Roke, S.; Bakker, H. J. Freezing effects of oil-in-water emulsions studied by sum-frequency scattering spectroscopy. *The Journal of Chemical Physics* **2016**, *145* (4), 044706. DOI: 10.1063/1.4959128.
(69) Carpenter, A. P.; Christoffersen, E. L.; Mapile, A. N.; Richmond, G. L. Assessing the Impact of Solvent Selection on Vibrational Sum-Frequency Scattering Spectroscopy Experiments. *The Journal of Physical Chemistry B* **2021**, *125* (12), 3216-3229. DOI: 10.1021/acs.jpcb.1c00188.

(70) Carpenter, A. P.; Foster, M. J.; Jones, K. K.; Richmond, G. L. Effects of Salt-Induced Charge Screening on AOT Adsorption to the Planar and Nanoemulsion Oil–Water Interfaces. *Langmuir* **2021**, *37* (29), 8658-8666. DOI: 10.1021/acs.langmuir.0c03606.
(71) Foster, M. J.; Carpenter, A. P.; Richmond, G. L. Dynamic Duo: Vibrational Sum Frequency Scattering Investigation of pH-Switchable Carboxylic Acid/Carboxylate Surfactants on Nanodroplet Surfaces. *The Journal of Physical Chemistry B* **2021**, *125* (33), 9629-9640. DOI: 10.1021/acs.jpcb.1c05508.
(72) Golbek, T. W.; Strunge, K.; Chatterley, A. S.; Weidner, T. Peptide Orientation at Emulsion Nanointerfaces Dramatically Different from Flat Surfaces. *The Journal of Physical Chemistry Letters* **2022**, *13* (46), 10858-10862. DOI: 10.1021/acs.jpclett.2c02870.
(73) Dadap, J. I.; Shan, J.; Eisenthal, K. B.; Heinz, T. F. Second-Harmonic Rayleigh Scattering from a Sphere of Centrosymmetric Material. *Physical Review Letters* **1999**, *83* (20), 4045-4048. DOI: 10.1103/PhysRevLett.83.4045.
(74) Yang, N.; Angerer, W. E.; Yodh, A. G. Angle-Resolved Second-Harmonic Light Scattering from Colloidal Particles. *Physical Review Letters* **2001**, *87* (10), 103902. DOI: 10.1103/PhysRevLett.87.103902.
(75) de Beer, A. G. F.; Roke, S. Nonlinear Mie theory for second-harmonic and sum-frequency scattering. *Physical Review B* **2009**, *79* (15), 155420. DOI: 10.1103/PhysRevB.79.155420.
(76) Beer, A. G. F. d.; Roke, S. Obtaining molecular orientation from second harmonic and sum frequency scattering experiments in water: Angular distribution and polarization dependence. *The Journal of Chemical Physics* **2010**, *132* (23), 234702. DOI: 10.1063/1.3429969.
(77) Qian, Y.; Brown, J. B.; Huang-Fu, Z.-C.; Zhang, T.; Wang, H.; Wang, S.; Dadap, J. I.; Rao, Y. In situ analysis of the bulk and surface chemical compositions of organic aerosol particles. *Communications Chemistry* **2022**, *5* (1), 58. DOI: 10.1038/s42004-022-00674-8.
(78) Qian, Y.; Brown, J. B.; Zhang, T.; Huang-Fu, Z.-C.; Rao, Y. In Situ Detection of Chemical Compositions at Nanodroplet Surfaces and In-Nanodroplet Phases. *The Journal of Physical Chemistry A* **2022**, *126* (23), 3758-3764. DOI: 10.1021/acs.jpca.2c03346.
(79) Marchioro, A.; Golbek, T. W.; Weidner, T.; Roke, S. Can vibrational sum frequency scattering spectra be measured from the surface of 40-100 nm aerosols in a cloud containing 10$^{6} $ particles/mL? *arXiv preprint arXiv:2206.01470* **2022**.
(80) Wang*, H.-F.; Gan, W.; Lu†‡ §, R.; Rao†‡¶, Y.; Wu, B.-H. Quantitative spectral and orientational analysis in surface sum frequency generation vibrational spectroscopy (SFG-VS). *International Reviews in Physical Chemistry* **2005**, *24* (2), 191-256. DOI: https://doi.org/10.1080/01442350500225894.
(81) Dadap, J. I.; Shan, J.; Heinz, T. F. Theory of optical second-harmonic generation from a sphere of centrosymmetric material: small-particle limit. *J. Opt. Soc. Am. B* **2004**, *21* (7), 1328-1347. DOI: 10.1364/JOSAB.21.001328.
(82) Wu, Y.; Li, W.; Xu, B.; Li, X.; Wang, H.; McNeill, V. F.; Rao, Y.; Dai, H.-L. Observation of organic molecules at the aerosol surface. *The Journal of Physical Chemistry Letters* **2016**, *7* (12), 2294-2297. DOI: https://doi.org/10.1021/acs.jpclett.6b00872.
(83) Qian, Y.; Deng, G.-h.; Rao, Y. In situ chemical analysis of the gas–aerosol particle interface. *Analytical chemistry* **2018**, *90* (18), 10967-10973. DOI: https://doi.org/10.1021/acs.analchem.8b02537.

(84) Ju, Y.; Fang, J.; Liu, X.; Xu, Z.; Ren, X.; Sun, C.; Yang, S.; Ren, Q.; Ding, Y.; Yu, K.; et al. Photodegradation of crystal violet in TiO2 suspensions using UV–vis irradiation from two microwave-powered electrodeless discharge lamps (EDL-2): Products, mechanism and feasibility. *Journal of Hazardous Materials* **2011**, *185* (2), 1489-1498. DOI: https://doi.org/10.1016/j.jhazmat.2010.10.074.
(85) Qian, Y.; Deng, G.-h.; Rao, Y. In situ spectroscopic probing of polarity and molecular configuration at aerosol particle surfaces. *The Journal of Physical Chemistry Letters* **2020**, *11* (16), 6763-6771. DOI: https://doi.org/10.1021/acs.jpclett.0c02013.
(86) Nathanson, G. M.; Davidovits, P.; Worsnop, D. R.; Kolb, C. E. Dynamics and Kinetics at the Gas−Liquid Interface. *The Journal of Physical Chemistry* **1996**, *100* (31), 13007-13020. DOI: 10.1021/jp953548e.
(87) Abbatt, J.; Lee, A.; Thornton, J. Quantifying trace gas uptake to tropospheric aerosol: recent advances and remaining challenges. *Chemical Society Reviews* **2012**, *41* (19), 6555-6581. DOI: https://doi.org/10.1039/C2CS35052A.
(88) Swenson, H.; Stadie, N. P. Langmuir's Theory of Adsorption: A Centennial Review. *Langmuir* **2019**, *35* (16), 5409-5426. DOI: 10.1021/acs.langmuir.9b00154.
(89) Castro, A.; Bhattacharyya, K.; Eisenthal, K. B. Energetics of adsorption of neutral and charged molecules at the air/water interface by second harmonic generation: Hydrophobic and solvation effects. *The Journal of Chemical Physics* **1991**, *95* (2), 1310-1315. DOI: 10.1063/1.461113.
(90) Qian, Y.; Deng, G.-h.; Lapp, J.; Rao, Y. Interfaces of Gas–Aerosol Particles: Relative Humidity and Salt Concentration Effects. *The Journal of Physical Chemistry A* **2019**, *123* (29), 6304-6312. DOI: https://doi.org/10.1021/acs.jpca.9b03896.
(91) Qian, Y.; Brown, J. B.; Wang, H.; Huang-Fu, Z.-C.; Zhang, T.; Narouei, F. H.; McNeill, V. F.; Rao, Y. Partitioning of Formic and Acetic Acids to the Gas/Aerosol Interface. *ACS Earth and Space Chemistry* **2023**, *7* (4), 885-891. DOI: 10.1021/acsearthspacechem.3c00024.
(92) Kolb, C. E.; Worsnop, D. R. Chemistry and Composition of Atmospheric Aerosol Particles. *Annual Review of Physical Chemistry* **2012**, *63* (1), 471-491. DOI: 10.1146/annurev-physchem-032511-143706 (acccessed 2023/03/21).
(93) Wokosin, K. A.; Schell, E. L.; Faust, J. A. Surfactants, Films, and Coatings on Atmospheric Aerosol Particles: A Review. *Environmental Science: Atmospheres* **2022**, *2*, 775-828. DOI: 10.1039/D2EA00003B.
(94) Steel, W. H.; Walker, R. A. Measuring dipolar width across liquid–liquid interfaces with 'molecular rulers'. *Nature* **2003**, *424* (6946), 296-299. DOI: https://doi.org/10.1038/nature01791.
(95) Yamaguchi, S.; Tahara, T. Precise Electronic χ(2) Spectra of Molecules Adsorbed at an Interface Measured by Multiplex Sum Frequency Generation. *The Journal of Physical Chemistry B* **2004**, *108* (50), 19079-19082. DOI: 10.1021/jp045306x.
(96) Watson, B. R.; Doughty, B.; Calhoun, T. R. Energetics at the Surface: Direct Optical Mapping of Core and Surface Electronic Structure in CdSe Quantum Dots Using Broadband Electronic Sum Frequency Generation Microspectroscopy. *Nano Letters* **2019**, *19* (9), 6157-6165. DOI: 10.1021/acs.nanolett.9b02201.
(97) Deng, G.-H.; Qian, Y.; Rao, Y. Development of ultrafast broadband electronic sum frequency generation for charge dynamics at surfaces and interfaces. *The Journal of Chemical Physics* **2019**, *150* (2), 024708. DOI: 10.1063/1.5063458.

(98) Zhang, T.; Huang-Fu, Z.-C.; Qian, Y.; Gao, H.; Brown, J. B.; Rao, Y. Photoinduced Surface Electric Fields and Surface Population Dynamics of GaP(100) Photoelectrodes. *The Journal of Physical Chemistry C* **2022**, *126* (14), 6531-6541. DOI: 10.1021/acs.jpcc.2c01806.
(99) Zhang, T.; Qian, Y.; Gao, H.; Huang-Fu, Z.-C.; Brown, J. B.; Rao, Y. Surface States for Photoelectrodes of Gallium Phosphide (GaP) with Surface-Specific Electronic Spectra and Phase Measurements. *The Journal of Physical Chemistry C* **2022**, *126* (15), 6761-6772. DOI: 10.1021/acs.jpcc.2c00412.
(100) Song, J. Second Harmonic Generation Study of Malachite Green Adsorption at the Interface between Air and an Electrolyte Solution: Observing the Effect of Excess Electrical Charge Density at the Interface. *The Journal of Physical Chemistry B* **2010**, *114* (9), 3236-3241. DOI: 10.1021/jp9104882.
(101) Yamaguchi, S.; Tahara, T. Development of Electronic Sum Frequency Generation Spectroscopies and Their Application to Liquid Interfaces. *The Journal of Physical Chemistry C* **2015**, *119* (27), 14815-14828. DOI: 10.1021/acs.jpcc.5b02375.
(102) Deng, G.-H.; Qian, Y.; Wei, Q.; Zhang, T.; Rao, Y. Interface-Specific Two-Dimensional Electronic Sum Frequency Generation Spectroscopy. *The Journal of Physical Chemistry Letters* **2020**, *11* (5), 1738-1745. DOI: 10.1021/acs.jpclett.0c00157.
(103) Lu, R.; Gan, W.; Wu, B.-h.; Zhang, Z.; Guo, Y.; Wang, H.-f. C−H Stretching Vibrations of Methyl, Methylene and Methine Groups at the Vapor/Alcohol (n = 1−8) Interfaces. *The Journal of Physical Chemistry B* **2005**, *109* (29), 14118-14129. DOI: 10.1021/jp051565q.
(104) Wang, S.; Zhao, Y.; Chan, A. W. H.; Yao, M.; Chen, Z.; Abbatt, J. P. D. Organic Peroxides in Aerosol: Key Reactive Intermediates for Multiphase Processes in the Atmosphere. *Chemical Reviews* **2023**, *123* (4), 1635-1679. DOI: 10.1021/acs.chemrev.2c00430.
(105) Stiopkin, I. V.; Jayathilake, H. D.; Bordenyuk, A. N.; Benderskii, A. V. Heterodyne-Detected Vibrational Sum Frequency Generation Spectroscopy. *Journal of the American Chemical Society* **2008**, *130* (7), 2271-2275. DOI: 10.1021/ja076708w.
(106) Xu, B.; Wu, Y.; Sun, D.; Dai, H.-L.; Rao, Y. Stabilized phase detection of heterodyne sum frequency generation for interfacial studies. *Opt. Lett.* **2015**, *40* (19), 4472-4475. DOI: 10.1364/OL.40.004472.
(107) Verreault, D.; Hua, W.; Allen, H. C. From Conventional to Phase-Sensitive Vibrational Sum Frequency Generation Spectroscopy: Probing Water Organization at Aqueous Interfaces. *The Journal of Physical Chemistry Letters* **2012**, *3* (20), 3012-3028. DOI: 10.1021/jz301179g.
(108) Rich, C. C.; Mattson, M. A.; Krummel, A. T. Direct Measurement of the Absolute Orientation of N3 Dye at Gold and Titanium Dioxide Surfaces with Heterodyne-Detected Vibrational SFG Spectroscopy. *The Journal of Physical Chemistry C* **2016**, *120* (12), 6601-6611. DOI: 10.1021/acs.jpcc.5b12649.
(109) Myalitsin, A.; Ghosh, S.; Urashima, S.-h.; Nihonyanagi, S.; Yamaguchi, S.; Aoki, T.; Tahara, T. Structure of water and polymer at the buried polymer/water interface unveiled using heterodyne-detected vibrational sum frequency generation. *Physical Chemistry Chemical Physics* **2020**, *22* (29), 16527-16531. DOI: https://doi.org/10.1039/D0CP02618B.
(110) Zhang, T.; Huangfu, Z.-C.; Qian, Y.; Lu, Z.; Gao, H.; Rao, Y. Spectral Phase Measurements of Heterodyne Detection in Interfacial Broadband Electronic Spectroscopy. *The Journal of Physical Chemistry C* **2022**, *126* (5), 2823-2832. DOI: 10.1021/acs.jpcc.1c09692.

TOC Graphic

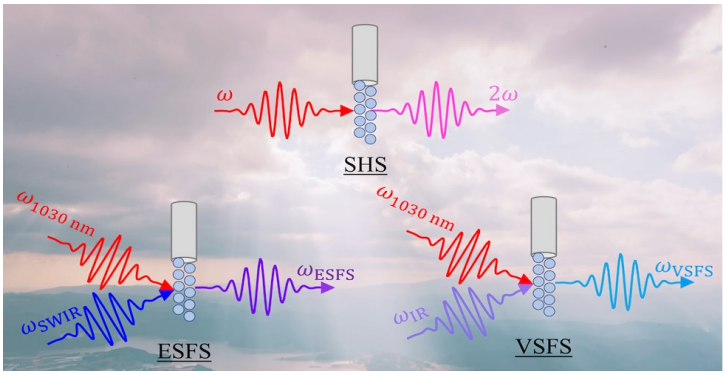

Biographies

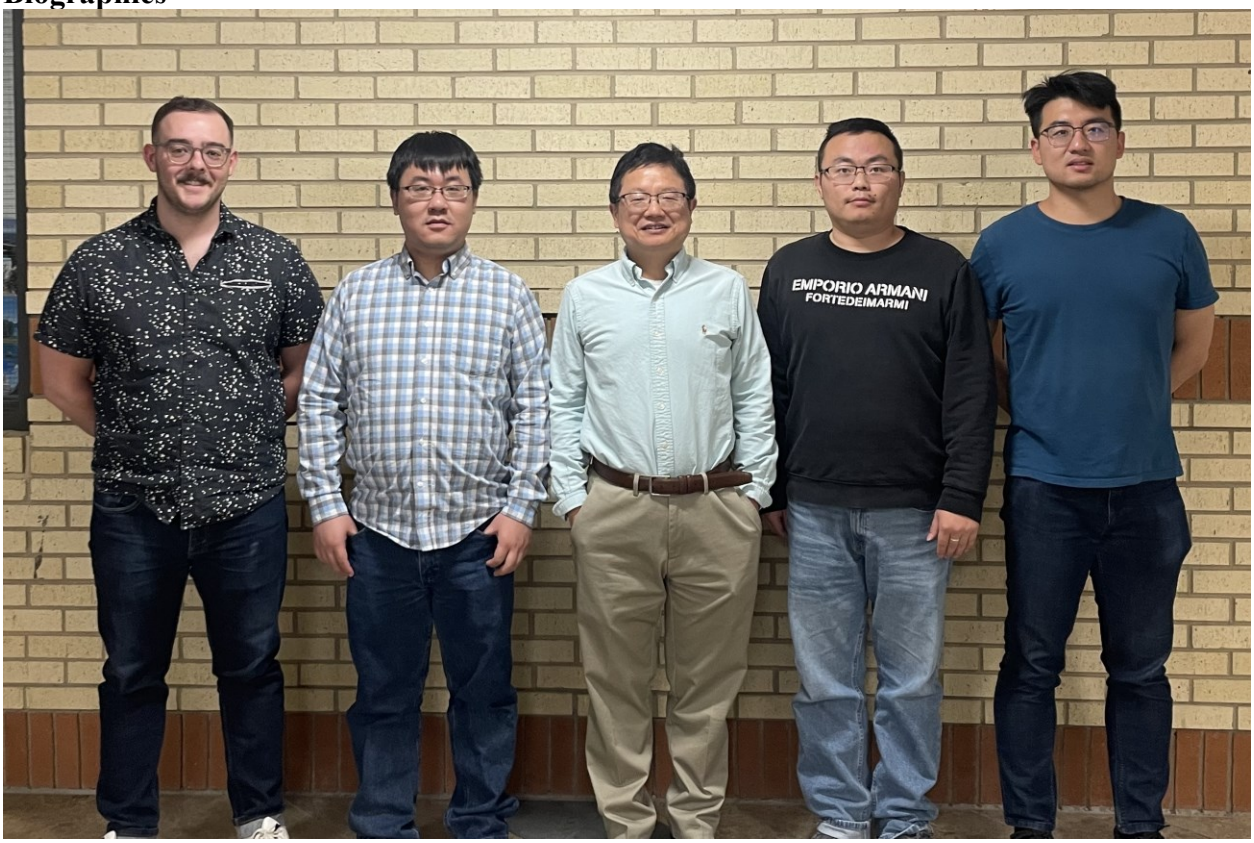

Authors (left to right): J.B.B., Y.Q., Y. R., H.W., and Z.-C. H.-F.

Jesse B. Brown received his B.S. in chemistry from Arkansas State University, AR, United States, and is now pursuing a Ph.D. in analytical chemistry at Utah State University, UT, United States in Prof. Yi Rao's group. Jesse's Ph.D. work is in the development of nonlinear optical scattering techniques for the investigation of atmospherically relevant properties and processes at aerosol particle surfaces. He plans to continue work in instrument development and aerosol research.

Yuqin Qian received his B.Sc. in chemistry from Temple University, PA, United States and later completed his Ph.D. in analytical chemistry at Utah State University, UT, United States in 2022. He is currently working as a post-doctoral researcher at Utah State University. His research interests include aerosol particle surfaces, sum frequency generation, and short-wave IR semiconductor materials.

Zhi-Chao Huang-Fu received his Ph.D. in physical chemistry at Xiamen University in 2019. He served as a research scientist (2019-2021) in the Department of Chemistry, College of Chemistry and Chemical Engineering, Xiamen University. He is currently working as a visiting scholar at Rao Group, Department of Chemistry and Biochemistry, Utah State University. His research interests include the development and application of ultrafast spectroscopies to improve our understanding of surfaces/interfaces, specifically the surfaces/interfaces in electrochemical systems.

Tong Zhang received her Ph.D. degree from the Institute of Chemistry, Chinese Academy of Science in 2022. During her doctorate, Tong was focused on surface states and their dynamics of photoelectrodes by developing heterodyne electronic sum frequency generation and time-resolved electronic sum frequency generation. Tong's research interest includes photoinduced interfacial dynamics, in situ detection of electrode surfaces, and surface reactions with interface-specific spectroscopies.

Hui Wang received his Ph.D. in physical chemistry from Fudan University. He is currently working on nonlinear optical scattering theory as well as the application of sum frequency generation to electrochemical systems as a visiting scholar in the Rao Group at Utah State University.

Yi Rao is a physical chemist with expertise in interfacial science, ultrafast spectroscopy, and nonlinear optics. Yi has obtained his PhD in 2003 at the Institute of Chemistry, Chinese Academy of Science. In 2004, he worked as a postdoctoral scientist at Columbia University. After his postdoc, Yi continued his career as a research associate at Columbia University. Before beginning his independent career, Yi worked as a research associate professor in the Department of Chemistry at Temple University in 2014. Yi joined the Department of Chemistry and Biochemistry at Utah State University as an assistant professor in 2017. His research interest is focused primarily on interfacial physical chemistry for environmental issues, solar energy conversion, and catalysis.